

MASTER THESIS

Numerical Method of Ultrasonic Welding Process

By

Apichan SRIPIEN

Supervised by

Prof. Steven LE CORRE

Arthur LEVY



CONTENTS

| | |
|--------------------------------|----|
| A. INTRODUCTION | 1 |
| B. PROCESS MODELLING | |
| Mechanical Problem | 2 |
| Thermal Problem | 3 |
| Time Homogenization | 3 |
| C. NUMERICAL APPROACH | |
| Simplification of equations | 8 |
| Geometry update | 9 |
| Resolution scheme | 9 |
| Test cases | 11 |
| D. PROCESS SIMULATION | |
| Geometry and meshing | 30 |
| Material properties | 31 |
| Boundary and initial condition | 31 |
| Results and discussion | 31 |
| E. Conclusion | 35 |
| F. References | 36 |

A. INTRODUCTION

A typical ultrasonic welding of thermoplastics is accomplished by applying frequency oscillation in the range of 10 to 40 kHz, oscillation amplitude usually range from 20 to 80 microns to the pieces to be joint together. The vibration energy is dissipated as heat that elevates the plastic temperature to a level sufficient to promote bonding between the pieces.

This work aims at modeling an original welding process of two composite material plates with thermoplastic matrix in 3D. The figure of the process can be shown in figure A.1.

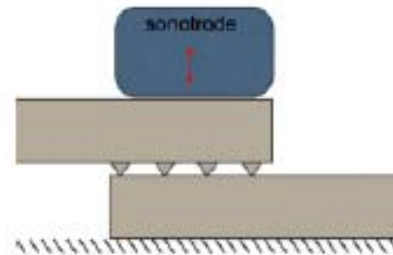


Figure A.1: Ultrasonic welding of two plates

Triangle energy directors are molded with matrix only, on the width of two centimeters on the border of one of the plate to be welded. The two plates are then positioned in order to cover each other on the width of the energy directors. The process starts when applying an ultrasonic sinusoidal frequency and amplitude by the sonotrode. Energy directors melt because of the viscous dissipation. The triangles then flow on the surfaces and weld the two plates together as shown in figure A.2.



Figure A.2: Melting and flowing of an energy director

The main difficulty of the modeling and simulation of this process comes from the existence of two different time scales. The first one will be “micro-chronological” that linked to short ultrasonic period. The second will be “macro-chronological”, which is the time of the process. Simulation each ultrasonic cycle would induce huge calculation times because the whole process performs over thousands of cycles. Time homogenization technique will be used to overcome this difficulty.

The final aim of this thesis is to perform simulation of “dynamic” welding instead of “static” welding where the sonotrode does not move on the plate. In our case, the sonotrode slides along the director direction and performs weld line. This makes three dimensional analysis become necessity.

B. PROCESS MODELING

Based on work of A. Levy, A. Poitou, S. Le Corre, E.Soccard, the process can be considered as Thermo-Mechanical problem since mechanical load given from sonotrode transfers into heat that melt and make energy directors flow. Let us consider one initial director as shown in figure B.1.

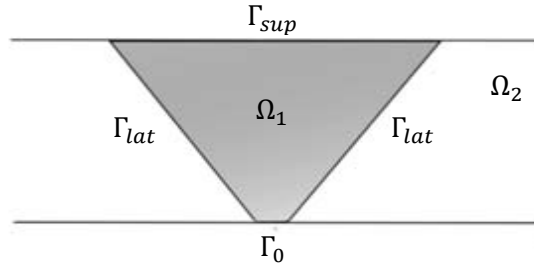


Figure B.1: Initial energy director

Mechanical Problem

In order to simplify the theoretical analysis, the material behaviour is first modeled by a linear Maxwell visco-elastic law:

$$\lambda \underline{\dot{\sigma}} + \underline{\sigma} = 2\eta \underline{\dot{\epsilon}}$$

where λ is the relaxation time, σ is the extra stress, η is the viscosity and D is the strain rate tensor. Both composite plates to be welded are supposed to be rigid compared to the director. The displacement at the tip of the director is considered to be zero. The displacement of the upper part can be split into two parts. One is “micro-chronological” sinusoidal displacement $a \cdot \sin(\omega t)$ which due to short period of ultrasound frequency. Another is “macro-chronological” displacement u_d which due to the squeezing of the director during the process. Finally the whole mechanical problem can be written as

$$\text{div}(\underline{\sigma} - p\underline{I}) = 0 \quad (1.1)$$

$$\lambda \underline{\dot{\sigma}} + \underline{\sigma} = 2\eta \underline{D} \quad (1.2)$$

$$\text{div}(\underline{u}) = 0 \quad (1.3)$$

with boundary condition $\underline{u} = \underline{u}_d(t) + \underline{a} \cdot \sin(\omega t)$ on Γ_{sup} (1.4)

$$(\underline{\sigma} - p\underline{I}) \cdot \underline{n} = 0 \quad \text{on } \Gamma_{lat} \quad (1.5)$$

$$\underline{u} = 0 \quad \text{on } \Gamma_0 \quad (1.6)$$

Thermal Problem

The director is supposed to be insulated. The viscous part of mechanical energy $\underline{\underline{\sigma}}: \underline{\underline{D}}_{vis}$ is supposed to be dissipated in the director during the process. Consider Maxwell's constitutive law, we can assume that $\underline{\underline{D}}_{vis} = \frac{1}{2\eta} \underline{\underline{\sigma}}$. So, the thermal equation can be written as

$$\rho c(\dot{\theta} + \underline{\underline{grad}}\theta \cdot \underline{\underline{v}}) = k\Delta\theta + \frac{1}{2\eta} \underline{\underline{\sigma}}: \underline{\underline{\sigma}} \quad (2.1)$$

$$\text{with boundary condition} \quad k \cdot \underline{\underline{grad}}\theta \cdot \underline{\underline{n}} = 0 \quad \text{on } \Gamma_{sup} \cup \Gamma_{lat} \cup \Gamma_0 \quad (2.2)$$

Time Homogenization

Introducing dimensionless time scales t^* and τ^* which represent macro-chronological time scale and micro-chronological time scale respectively. We can define $t = \lambda_0 t^*$ and $\tau^* = \omega t$, where $\lambda_0 = 1 \text{ s}$ which is characteristic time of the process.

$$\text{Then we can clarify the scale factor} \quad \xi = \frac{t^*}{\tau^*} = \frac{1}{\omega \lambda_0} \approx 10^{-6} \quad (3)$$

The two time scales are well separated. This will allow us to use a technique of homogenization in time to model the process. Each variable ϕ of the problem is written as a function of time t^* and τ^* . The time derivative of ϕ can be written as

$$\dot{\phi} = \frac{d\phi}{dt} = \frac{1}{\lambda_0} \frac{\partial \phi}{\partial t^*} + \frac{1}{\lambda_0} \frac{1}{\xi} \frac{\partial \phi}{\partial \tau^*} \quad (4)$$

Presenting other dimensionless variables

$$\underline{\underline{\sigma}} = \frac{\eta_0}{\lambda_0} \underline{\underline{\sigma}}^* \quad (5.1)$$

$$\underline{\underline{\varepsilon}} = \underline{\underline{\varepsilon}}^* \quad (5.2)$$

$$\underline{\underline{\varepsilon}} = \underline{\underline{grad}}_s^* \underline{\underline{u}}^* \quad (5.3)$$

$$\underline{\underline{u}} = e \underline{\underline{u}}^* \quad (5.4)$$

where η_0 and e are characteristic viscosity and characteristic length of the problem.

Also introducing dimensionless space operators

$$\underline{\underline{grad}} \equiv \frac{1}{e} \underline{\underline{grad}}^* \quad (6.1)$$

$$\underline{\underline{div}} \equiv \frac{1}{e} \underline{\underline{div}}^* \quad (6.2)$$

$$\Delta \equiv \frac{1}{e^2} \Delta^* \quad (6.3)$$

By injecting equations (4) and (5) into equation (1.2) and (1.4), we have dimensionless equations

$$\lambda^* \frac{\partial \underline{\underline{\sigma}}^*}{\partial t^*} + \lambda^* \frac{1}{\xi} \frac{\partial \underline{\underline{\sigma}}^*}{\partial \tau^*} + \underline{\underline{\sigma}}^* = 2\eta^* \frac{\partial \underline{\underline{\varepsilon}}^*}{\partial t^*} + 2\eta^* \frac{1}{\xi} \frac{\partial \underline{\underline{\varepsilon}}^*}{\partial \tau^*} \quad (7.1)$$

$$\underline{\underline{u}}^* = \underline{\underline{u}}^*_d(t^*) + \underline{\underline{R}} \sin(\tau^*) \text{ on } \Gamma_{sup} \quad (7.2)$$

Quantity R is of order 0 in ξ .

Asymptotic expansion in time consists in writing each unknown as an expansion in power of ξ

$$\phi^* = \phi_0^* + \phi_1^* \xi + \phi_2^* \xi^2 + \dots \quad (8)$$

where each ϕ^* is periodic in τ .

To simplify the mechanical problem, terms of velocity will replace displacements. In time derivation frame work the velocity is defined by

$$\underline{\underline{v}}^* = \frac{\partial \underline{\underline{u}}^*}{\partial t^*} + \frac{1}{\xi} \frac{\partial \underline{\underline{u}}^*}{\partial \tau^*} \quad (9)$$

which means that the velocity expansion start at order -1 with

$$\underline{\underline{v}}^*_{-1} = \frac{\partial \underline{\underline{u}}^*_0}{\partial \tau^*} \quad (10.1)$$

$$\underline{\underline{v}}^*_i = \frac{\partial \underline{\underline{u}}^*_i}{\partial t^*} + \frac{\partial \underline{\underline{u}}^*_{i+1}}{\partial \tau^*} \quad \forall i \geq 0 \quad (10.2)$$

Strain rate can be expanded in the same way

$$\underline{\underline{D}}^*_{-1} = \text{grad}_s^*(\underline{\underline{v}}^*_{-1}) = \frac{\partial \underline{\underline{\varepsilon}}^*_0}{\partial \tau^*} \quad (11.1)$$

$$\underline{\underline{D}}^*_i = \text{grad}_s^*(\underline{\underline{v}}^*_i) = \frac{\partial \underline{\underline{\varepsilon}}^*_i}{\partial t^*} + \frac{\partial \underline{\underline{\varepsilon}}^*_{i+1}}{\partial \tau^*} \quad (11.2)$$

Identification of different order of ξ leads to a whole set of equations. First, we can notice that the equilibrium equation (1.1), incompressibility constraint (1.3) and two boundary conditions (1.5 and 1.6) can be identified trivially at every order i of ξ .

$$\text{div}^*(\underline{\underline{\sigma}}^*_i - p_i^* \underline{\underline{I}}) = 0 \quad (12.1)$$

$$\text{div}^*(\underline{\underline{u}}^*_i) = 0 \quad (12.2)$$

$$\text{boundary conditions} \quad \underline{\underline{u}}^*_i = 0 \quad \text{on } \Gamma_0 \quad (12.3)$$

$$(\underline{\underline{\sigma}}^*_i - p_i^* \underline{\underline{I}}) \cdot \underline{\underline{n}} = 0 \quad \text{on } \Gamma_{lat} \quad (12.4)$$

or in term of velocity

$$div^* (\underline{\underline{\sigma}}_i^* - p_i^* \underline{\underline{l}}) = 0 \quad (13.1)$$

$$div^* (\underline{\underline{v}}_i^*) = 0 \quad (13.2)$$

$$\text{boundary conditions} \quad \underline{\underline{v}}_i^* = 0 \quad \text{on } \Gamma_0 \quad (13.3)$$

$$(\underline{\underline{\sigma}}_i^* - p_i^* \underline{\underline{l}}) \cdot \underline{\underline{n}} = 0 \quad \text{on } \Gamma_{lat} \quad (13.4)$$

The displacement boundary condition on Γ_{sup} (7.2) only appear at order 0 as

$$\underline{\underline{u}}_i^* = 0 \quad \text{on } \Gamma_{sup} \quad (14.1)$$

$$\underline{\underline{u}}_0^* = \underline{\underline{u}}_d^*(t^*) + \underline{\underline{R}} \sin(\tau^*) \quad \text{on } \Gamma_{sup} \quad (14.2)$$

or in term of velocity

$$\underline{\underline{v}}_{-1}^* = \frac{\partial \underline{\underline{u}}_0^*}{\partial \tau^*} = \underline{\underline{R}} \cos(\tau^*) \quad \text{on } \Gamma_{sup} \quad (15.1)$$

$$\underline{\underline{v}}_0^* = \frac{\partial \underline{\underline{u}}_0^*}{\partial t^*} + \frac{\partial \underline{\underline{u}}_1^*}{\partial \tau^*} = \frac{\partial \underline{\underline{u}}_d^*}{\partial t^*} \quad \text{on } \Gamma_{sup} \quad (15.2)$$

$$\underline{\underline{v}}_i^* = 0 \quad \text{on } \Gamma_{sup} \quad (15.3)$$

Then Maxwell's constitutive law is identified as

$$\text{order } \xi^{-1}: \quad \lambda^* \frac{1}{\xi} \frac{\partial \underline{\underline{\sigma}}_0^*}{\partial \tau^*} = 2\eta^* \frac{\partial \underline{\underline{\varepsilon}}_0^*}{\partial \tau^*} = 2\eta^* \underline{\underline{D}}_{-1}^* \quad (16)$$

$$\text{order } \xi^0: \quad \lambda^* \frac{\partial \underline{\underline{\sigma}}_0^*}{\partial t^*} + \lambda^* \frac{1}{\xi} \frac{\partial \underline{\underline{\sigma}}_1^*}{\partial \tau^*} + \underline{\underline{\sigma}}_0^* = 2\eta^* \frac{\partial \underline{\underline{\varepsilon}}_0^*}{\partial t^*} + 2\eta^* \frac{\partial \underline{\underline{\varepsilon}}_1^*}{\partial \tau^*} \quad (17)$$

Introducing short time average operator $\langle \cdot \rangle = \frac{1}{|\kappa|} \int_{\kappa} (\cdot) d\tau$ where κ is the ultrasonic period.

Periodicity of $\underline{\underline{\sigma}}_i$ implies $\langle \frac{\partial \underline{\underline{\sigma}}_i^*}{\partial \tau^*} \rangle = 0$. Equation (17) becomes

$$\lambda^* \frac{\partial \langle \underline{\underline{\sigma}}_0^* \rangle}{\partial t^*} + \langle \underline{\underline{\sigma}}_0^* \rangle = 2\eta^* \frac{\partial \langle \underline{\underline{\varepsilon}}_0^* \rangle}{\partial t^*} \quad (18)$$

Finally, combining constitutive equations (16) and (18), equilibrium, incompressibility constrain and boundary conditions (13) and (15), we can separate mechanical problem into two different time scales.

1.) Micro-chronological mechanical problem

$$\lambda^* \frac{1}{\xi} \frac{\partial \underline{\underline{\sigma}}_0^*}{\partial \tau^*} = 2\eta^* \underline{\underline{D}}_{-1}^* \quad (19.1)$$

$$div^* (\underline{\underline{\sigma}}_0^* - p_0^* \underline{\underline{l}}) = 0 \quad (19.2)$$

$$div^*(\underline{v}_{-1}^*) = 0 \quad (19.3)$$

$$\text{boundary conditions} \quad \underline{v}_{-1}^* = \underline{R} \cos(\tau^*) \quad \text{on } \Gamma_{sup} \quad (19.4)$$

$$\underline{v}_{-1}^* = 0 \quad \text{on } \Gamma_0 \quad (19.5)$$

$$(\underline{\sigma}_0^* - p_0^* \underline{I}) \cdot \underline{n} = 0 \quad \text{on } \Gamma_{lat} \quad (19.6)$$

It is a hypo-elastic problem which is equivalent to elastic problem in the small displacement framework. This deals with short time period τ^* . The velocity conditions come from order ξ^{-1} . The boundary condition on Γ_{sup} is the micro-chronological harmonic condition only.

2.) Macro-chronological mechanical problem

$$\lambda^* \frac{\partial \langle \underline{\sigma}_0^* \rangle}{\partial t^*} + \langle \underline{\sigma}_0^* \rangle = 2\eta^* \frac{\partial \langle \underline{\varepsilon}_0^* \rangle}{\partial t^*} \quad (20.1)$$

$$div^*(\langle \underline{\sigma}_0^* \rangle - \langle p_0^* \rangle \underline{I}) = 0 \quad (20.2)$$

$$\text{boundary conditions} \quad \langle \underline{v}_0^* \rangle = \underline{v}_d^*(t^*) \quad \text{on } \Gamma_{sup} \quad (20.3)$$

$$\langle \underline{v}_0^* \rangle = 0 \quad \text{on } \Gamma_0 \quad (20.4)$$

$$(\langle \underline{\sigma}_0^* \rangle - \langle p_0^* \rangle \underline{I}) \cdot \underline{n} = 0 \quad \text{on } \Gamma_{lat} \quad (20.5)$$

This is a visco-elastic flow which deal with process time period t^* . The boundary condition on Γ_{sup} is the macro-chronological part only.

3.) Thermal problem

Introducing dimensionless temperature θ^* such that

$$\theta^* = \frac{\theta - \theta_{amb}}{\theta_{ref}} \quad (21)$$

Starting from equation (2), apply same analysis as mechanical problem. The boundary condition is trivially identified at every order of ξ as

$$\underline{grad}^*(\theta_i^*) \cdot \underline{n} = 0 \quad \text{on } \Gamma_{sup} \cup \Gamma_{lat} \cup \Gamma_0 \quad (22)$$

The thermal equation (2.1) can be identified at order ξ^{-1} as

$$\frac{\partial \theta_0^*}{\partial \tau^*} = 0 \quad (23)$$

which implies that $\langle \theta_0^* \rangle = \theta_0^*(t^*)$

and at order ξ^0 , we have

$$\frac{\partial \theta_0^*}{\partial t} + \frac{\partial \theta_1^*}{\partial \tau^*} + \underline{grad}^* \theta_0^* \cdot \underline{v}^* = A \Delta^* \theta_0^* + B \underline{\sigma}_0 : \underline{\sigma}_0 \quad (24)$$

Averaging over ultrasonic period, finally we get

$$\frac{\partial \theta_0^*}{\partial t} + \underline{\underline{grad}}^* \theta_0^* \cdot \underline{\underline{v}}^* = A \Delta^* \theta_0^* + B \langle \underline{\underline{\sigma}}_0 : \underline{\underline{\sigma}}_0 \rangle \quad (25.1)$$

$$\text{with boundary condition } \underline{\underline{grad}}^*(\theta_0^*) \cdot \underline{\underline{n}} = 0 \quad \text{on } \Gamma_{sup} \cup \Gamma_{lat} \cup \Gamma_0 \quad (25.2)$$

where A and B can be computed from thermal parameters and be found of order 0 in ξ .

Time homogenization technique allows us to split the initial multi time scale thermo-mechanical problem into three single time scale systems of equations, two mechanical problems coupling with one thermal problem. The micro-chronological mechanical problem induces source term in the thermal problem and macro-chronological mechanical problem will provide geometry change of the energy director. The thermal problem gives temperature which is needed for updating temperature dependent properties of material when solving both mechanical problems.

C. NUMERICAL APPROACH

As shown in previous section, instead of solving complex mechanical visco-elastic problem, time homogenization allows us to split the visco-elastic problem into two simple mechanic problems. One is micro chronological problem which is elastic like problem that will provide heat source to the thermal problem. Although macro chronological problem should be visco-elastic, for simplicity, it was set to purely viscous problem which will provide geometry update. Doing so, on the one hand we neglect the effects of elasticity on the macroscopic shape changes, but on the other hand we can introduce more easily the non-Newtonian behavior (rate dependent viscosity) which will lead to more realistic shape evolutions than a linear approximation. The thermal problem is solved to update thermal dependent properties of the energy director.

Simplification of the equations

1) Micro chronological problem (Elastic problem)

$$\text{Equilibrium equation: } \underline{\underline{div}}(\underline{\underline{\sigma}}) = \underline{\underline{0}} \quad (26.1)$$

$$\text{Constitutive equation: } \underline{\underline{\sigma}} = \underline{\underline{C}} : \underline{\underline{\varepsilon}} \quad (26.2)$$

$$\text{Strain-displacement relation: } \underline{\underline{\varepsilon}} = \frac{1}{2} [\underline{\underline{grad}}(\underline{\underline{u}}) + \underline{\underline{grad}}^T(\underline{\underline{u}})] \quad (26.3)$$

$$\text{Boundary conditions: } \underline{\underline{\sigma}} \cdot \underline{\underline{n}} = \underline{\underline{t}} \quad \text{on } \Gamma_\sigma \quad (26.4)$$

$$\underline{\underline{u}} = \underline{\underline{u}} \quad \text{on } \Gamma_u \quad (26.5)$$

2) Macro chronological problem (Fluid mechanic like problem)

$$\text{Equilibrium equation: } \underline{\underline{div}}(\underline{\underline{\sigma}} - p\underline{\underline{I}}) = \underline{\underline{0}} \quad (27.1)$$

$$\text{Incompressibility: } \underline{\underline{div}}(\underline{\underline{v}}) = 0 \quad (27.2)$$

$$\text{Constitutive equation: } \underline{\underline{\sigma}} = 2\underline{\underline{\eta}}\underline{\underline{D}} \quad (27.3)$$

$$\text{Strain rate tensor: } \underline{\underline{D}} = \frac{1}{2} (\underline{\underline{\nabla}}\underline{\underline{v}} + \underline{\underline{\nabla}}\underline{\underline{v}}^T) \quad (27.4)$$

$$\text{Boundary conditions: } \underline{\underline{t}} = p\underline{\underline{n}} \quad \text{on } \Gamma_t \quad (27.5)$$

$$\underline{\underline{v}} = \underline{\underline{v}} \quad \text{on } \Gamma_v \quad (27.6)$$

$$\text{Initial condition: } \underline{\underline{v}}_{t=0} = \underline{\underline{v}}^{(0)} \quad \text{in } \Omega \quad (27.7)$$

3) Thermal problem

$$\text{Heat transfer equation: } \rho c \left(\dot{T} + \underline{\underline{grad}}T \cdot \underline{\underline{v}} \right) - k \Delta T = q_{gen} \quad (28.1)$$

$$\text{Boundary conditions: } -\underline{\underline{q}} \cdot \underline{\underline{n}} = q \quad \text{on } \Gamma_q \quad (28.2)$$

$$T = T \quad \text{on } \Gamma_T \quad (28.3)$$

$$\text{Initial condition: } T_{t=0} = T^{(0)} \quad \text{on } \Omega \quad (28.4)$$

Where q_{gen} is the thermal source induced by micro chronological problem as the term $B < \underline{\underline{\sigma}}_0 : \underline{\underline{\sigma}}_0 >$ in (25.1).

To solve thermal problem, we will use operator splitting technique to separate diffusion convection heat transfer problem to one diffusion problem and one convection problem. For each time step, first, solve diffusion equation by using $T_{t=t_n} = T^n$ as an initial condition and then use T^* which is solved by diffusion equation as an initial condition for solving convection equation.

3.1) Thermal diffusion problem

$$\begin{aligned} \rho c \dot{T} - k \Delta T &= q_{gen} & (28.5) \\ \text{initial condition: } T_{t=t_n} &= T^n \\ &\Rightarrow T^* \end{aligned}$$

3.2) Thermal convection problem

$$\begin{aligned} \rho c (\underline{grad} T \cdot \underline{v}) &= 0 & (28.6) \\ \text{initial condition: } T_{t=t_n} &= T^* \\ &\Rightarrow T^{n+1} \end{aligned}$$

Geometry update

The ultrasonic welding model is concerned with deformation of energy director which is provided from solving macro chronological problem. We use the XFEM (extended finite element method) and level set approach to capture interface Γ of the energy director. The approach consists in specifying a continuous “level set function” Φ such that Φ is the signed distance to the interface Γ , $\Phi < 0$ in Ω_1 and $\Phi > 0$ in Ω_2 . The interface of the director can be described by $\Gamma = \{x | \Phi(x, t) = 0 \forall t \geq 0\}$ and $|\nabla \Phi| = 1$ in Ω

The evolution of the level set can be found from

$$\frac{\partial \Phi}{\partial t} + \underline{v} \cdot \nabla \Phi = 0 \quad \text{in } \Omega, t > 0 \quad (29)$$

Where \underline{v} is the solution of macro chronological fluid mechanic like problem. To stabilize the problem CFL condition is then selected under constraint of $Co \leq \frac{1}{2}$ ($Co = \frac{|\underline{v}| \Delta t}{h}$). So, during one time step the interface does not move further than to the distance $\frac{1}{2}h$ from its previous position. The time step is selecting under constrain of this condition.

Resolution scheme

Each system of equations is solved successively using a classic Galerkin FEM except the thermal convection problem. Reference to *A. N. Brooks and T.J.R. Hughes*, The SUPG (Streamline-Upwind Petrov-Galerkin) method is used as a stabilization technique for convection equation. Each problem which can be non-linear is solved by Newton-Raphson method. The global procedure is explicit in time, but thermal problem is solved by implicit backward Euler method. The elastic problem is treated using second order interpolation for displacements. Second order for temperature is also set in thermal problem. The fluid

problem is solved by second order for velocities and first order for pressure in order to satisfy the LBB conditions (*I. Babuska*). It is known as P2/P1 interpolation.

Our computational approach for numerical modeling of ultrasonic welding can be summarized as follows.

Step 0. Initialize the levelset function and velocity.

For each n-th time step, $n = 1, 2, 3, \dots$:

1. Solve micro chronological mechanical system equations.
2. Solve macro chronological thermal diffusion equations.
3. Solve macro chronological mechanical problem.
4. Geometry update
5. Solve macro chronological thermal convection equations.

The steps 1-3 are performed iteratively until the residual of all three problems are simultaneously smaller than a prescribed tolerance. This will ensure that all solutions are converged before evolution of the geometry. Time increment for each step is computed by CFL condition of geometry update step.

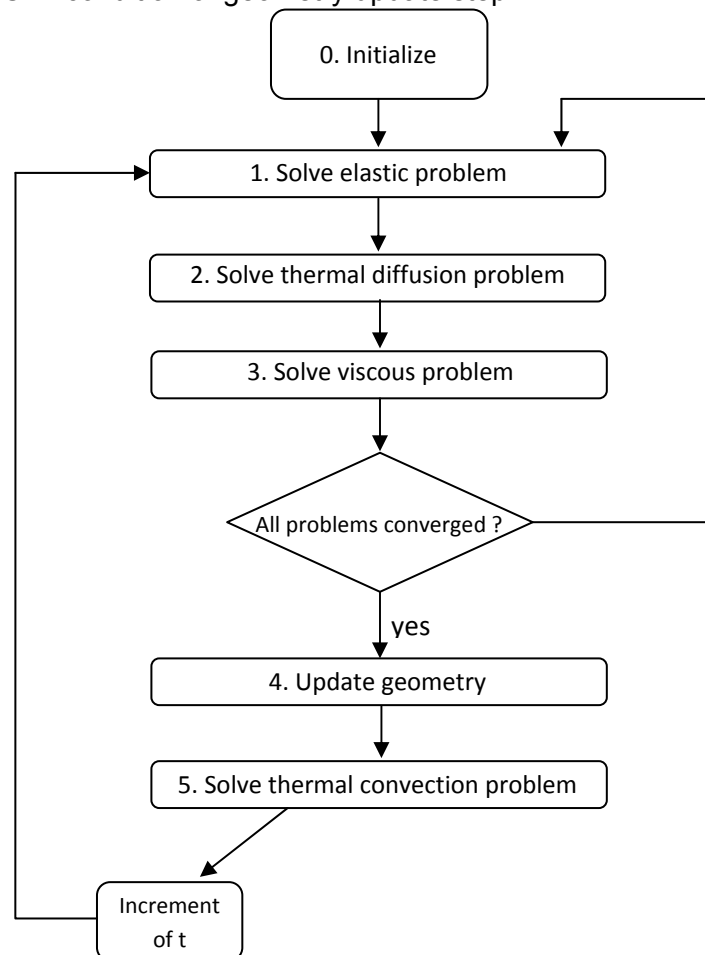


Figure C.1: Resolution Scheme Flow Chart

The resolution is performed on a fixed mesh where the interface is described by a level set function as mentioned before. The code is done using C++ Library X-FEM. Pre and post processing are using Gmsh^[1] software.

^[1] <http://geuz.org/gmsh/>

Test cases

Before modeling the ultrasonic welding process by above proposed numerical approach, some simple test cases are needed to be done to validate that our codes can solve each system of equations correctly.

1) Elastic test case

Simple shear test case

Determine a cube with given boundary conditions:

$$u_x(y = 1) = 1, u_x(y = 0) = 0, u_y = 0 \text{ and } u_z = 0$$

The problem becomes a simple shear. Displacement has only one component in x direction and is linear with y ($\frac{\partial u_x(y)}{\partial y} = \text{const}$). Using prescribed displacement on the top and bottom will give $u_x = 0.5y + 0.5$ and $\frac{\partial u_x(y)}{\partial y} = \varepsilon_{xy} = 0.5$. For material with young modulus $E = 3 \times 10^9 \text{ Pa}$ and Poisson's ratio $\nu = 0.3$, σ_{xy} can be calculated by

$$\sigma_{xy} = \frac{E}{2(1+\nu)} \varepsilon_{xy} = 5.78 \times 10^8 \text{ Pa}.$$

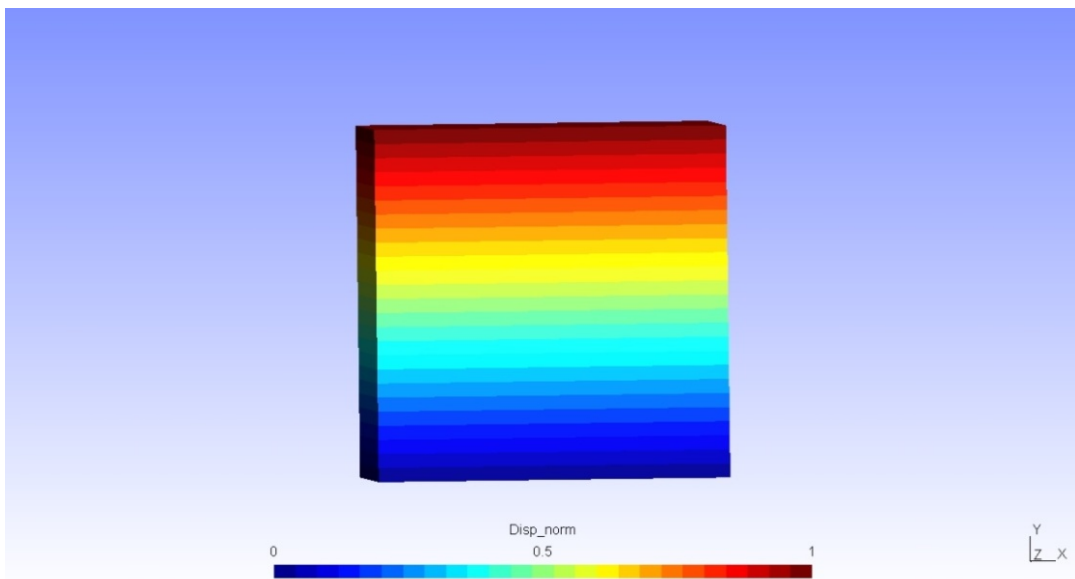


Figure C.2: Simple shear test case result: displacement

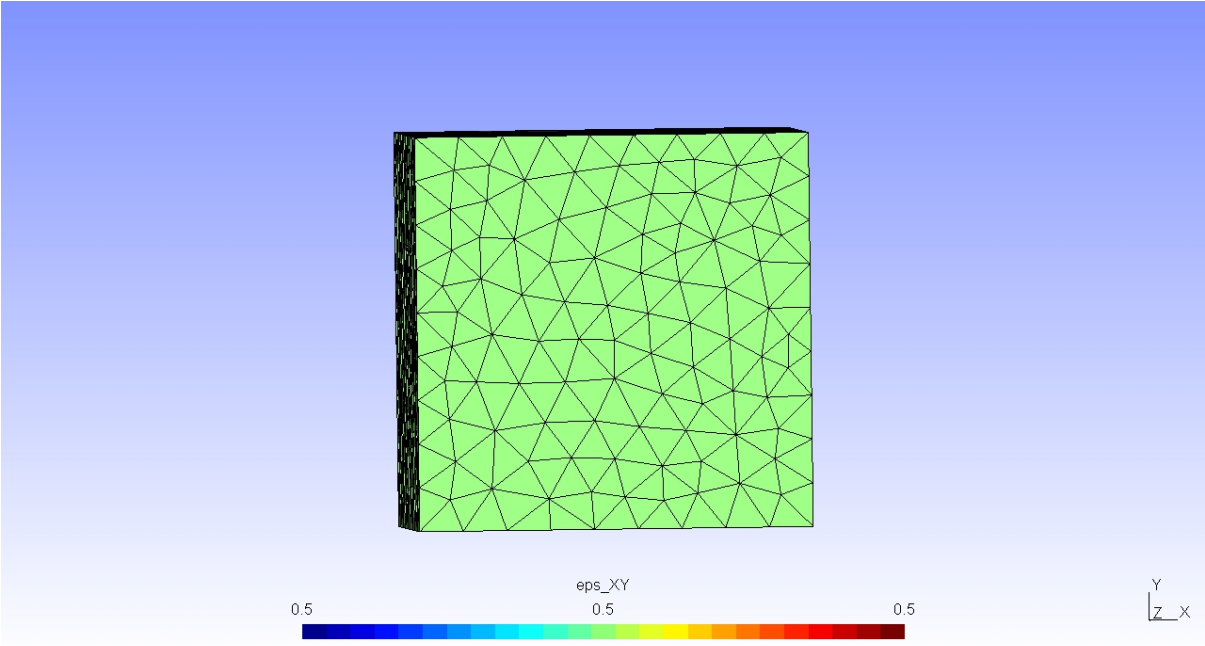


Figure C.3: Simple shear test case result: $\epsilon_{xy} = 0.5$

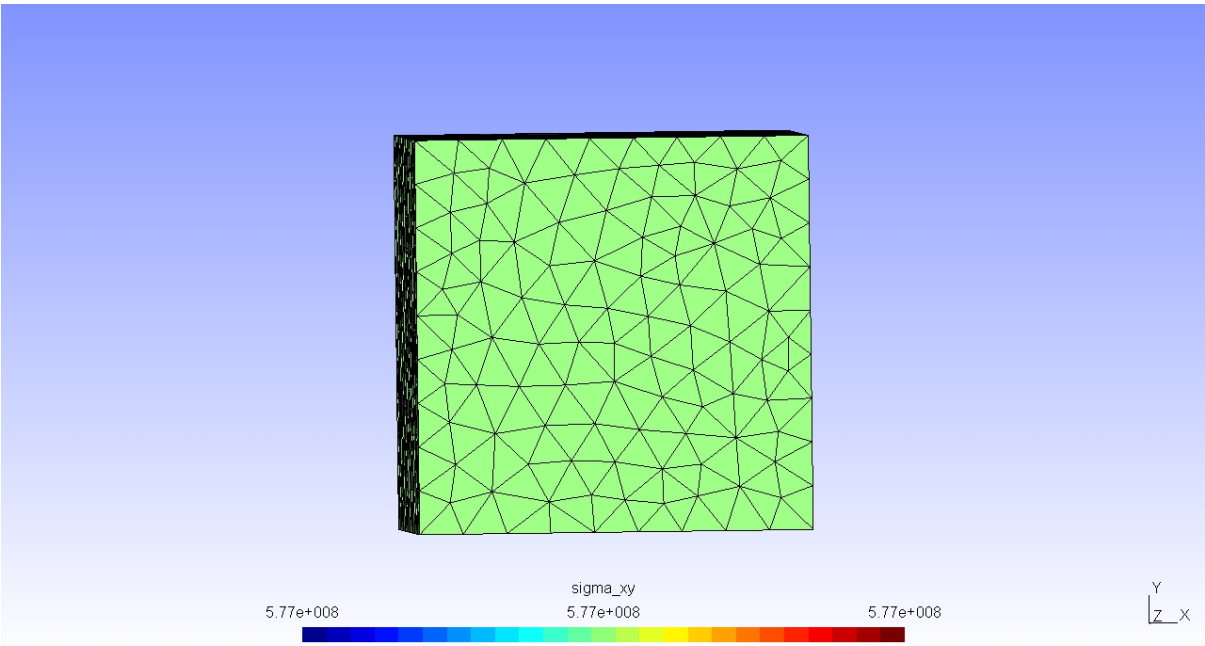


Figure C.4: Simple shear test case result: $\sigma_{xy} = 5.77 \times 10^8 \text{ Pa}$

For Newtonian fluid which has viscosity $0.02 \text{ Pa} \cdot \text{s}$ will give $p = 0.01 \text{ Pa}$,

$$\underline{\underline{\sigma}} = \begin{bmatrix} 0.01 & 0 & 0 \\ 0 & -0.02 & 0 \\ 0 & 0 & 0.01 \end{bmatrix} \text{ and } \underline{\underline{\Sigma}} = \begin{bmatrix} 0 & 0 & 0 \\ 0 & -0.03 & 0 \\ 0 & 0 & 0 \end{bmatrix} \text{ where } \underline{\underline{\Sigma}} = \underline{\underline{\sigma}} - p\underline{\underline{I}} \text{ is the total stress tensor.}$$

- **Numerical solutions**

The results of the problems using X-FEM by pre and post processing by Gmsh can be shown as below:

- Newtonian Fluid with viscosity $0.02 \text{ Pa} \cdot \text{s}$

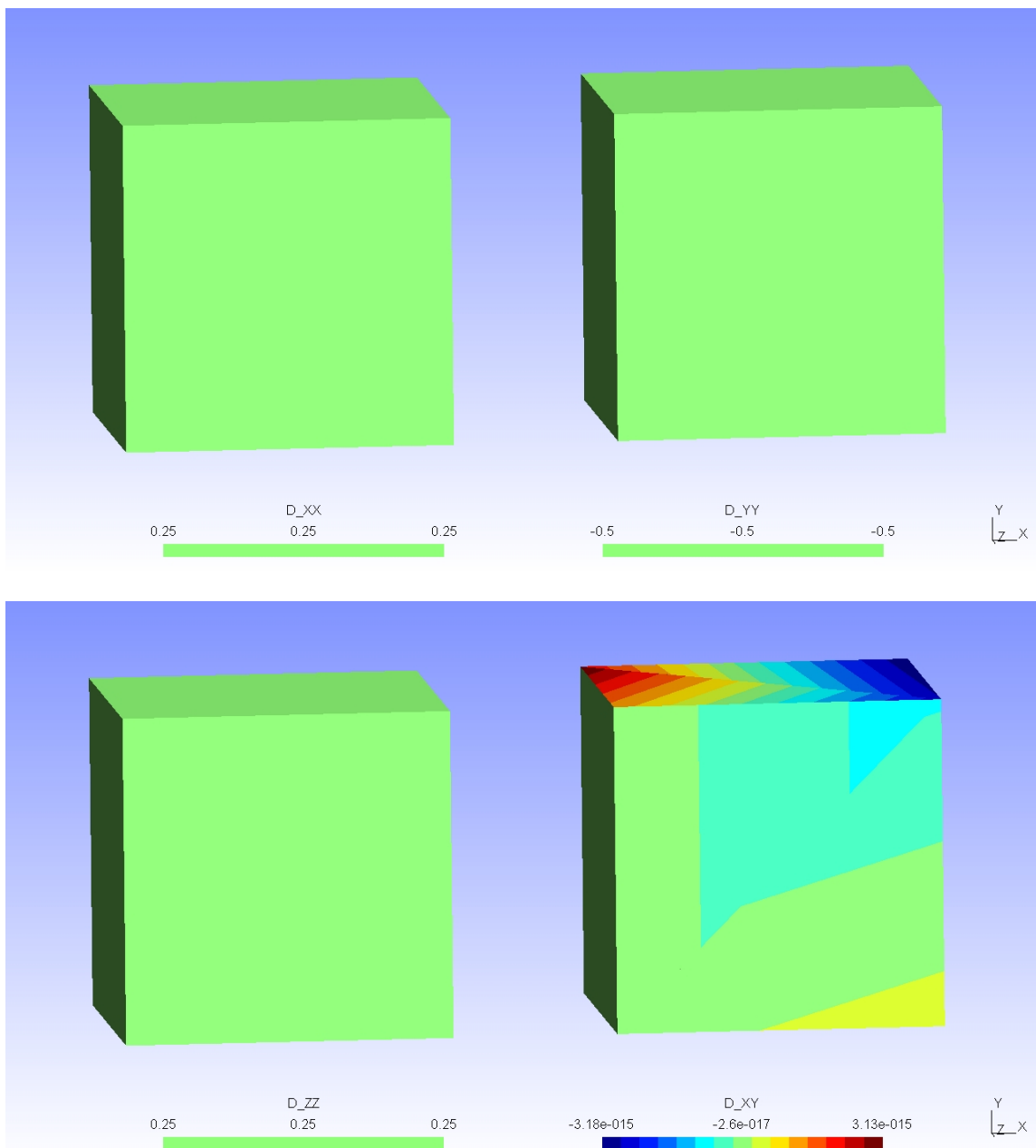


Figure C.6: Homogeneous test case result: Strain rate tensor component

The figure shows that D_{xx} , D_{yy} and D_{zz} are exactly the same values as the analytical solution. The D_{xy} is a very small value which comes from numerical error. Pressure and stress tensor components also can be extracted from the numerical solution and it gives the correct value compare with the analytical as shown below.

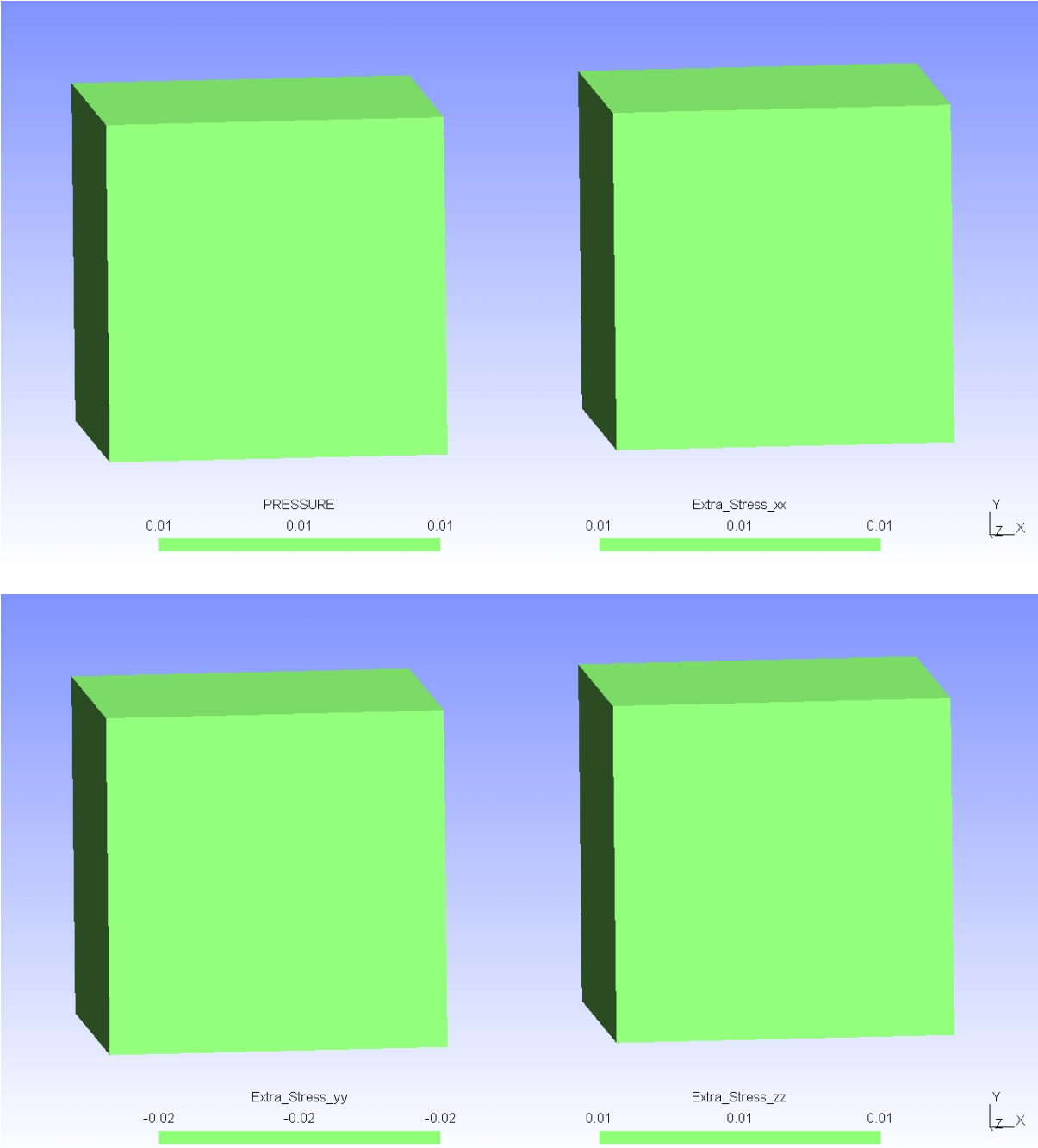


Figure C.7: Homogeneous test case result: Pressure, Extra stress components

2.2) Poiseuille flow test case

Consider incompressible flow in rectangular pipe of length $2L$, and square cross section wide $2H$ with given constant pressure at the inlet and outlet of the pipe p_{in} and p_{out} . By imposing no velocity flux going out ($\underline{v} \cdot \underline{n} = 0$) and inviscid flow at the front and back side of the tube (plane $z = \pm H$). The problem will act like 2D flow between 2 plates.

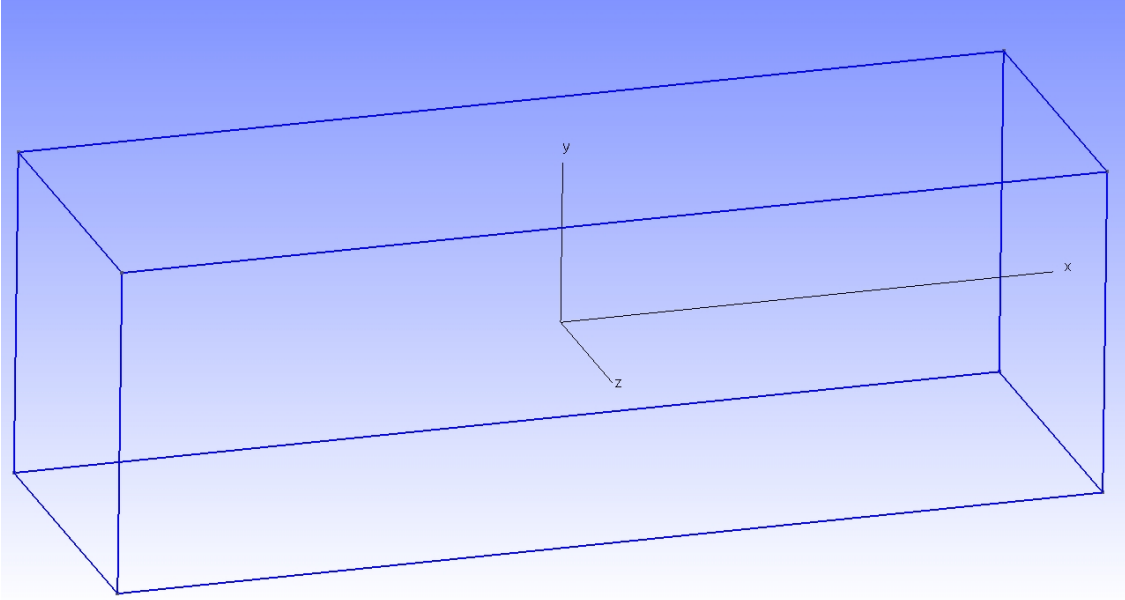


Figure C.8: Poiseuille flow test case

From equilibrium equations, we have

$$\text{div} (\underline{\underline{\sigma}} - p\underline{\underline{1}}) = \underline{0} \quad \text{or} \quad \sigma_{ij,j} + p_{,i} = 0 \quad (30)$$

$$\begin{cases} \sigma_{xx,x} + \sigma_{xy,y} - p_{,x} = 0 \\ \sigma_{yx,x} + \sigma_{yy,y} - p_{,y} = 0 \end{cases}$$

Assuming a velocity field of the form $\underline{v} = \begin{Bmatrix} v_x(y) \\ 0 \\ 0 \end{Bmatrix}$, then strain rate tensor $\underline{\underline{D}}$ and extra stress tensor $\underline{\underline{\sigma}}$ will left only xy component.

$$\underline{\underline{D}} = \begin{bmatrix} 0 & \frac{1}{2}v_{x,y} & 0 \\ \frac{1}{2}v_{x,y} & 0 & 0 \\ 0 & 0 & 0 \end{bmatrix} \quad \text{and} \quad \underline{\underline{\sigma}} = \begin{bmatrix} 0 & \sigma_{xy} & 0 \\ \sigma_{xy} & 0 & 0 \\ 0 & 0 & 0 \end{bmatrix} \quad (31)$$

Because $\underline{\underline{\sigma}} = 2\eta\underline{\underline{D}}$ and $\underline{\underline{D}}$ is only a function of y , we have $\sigma_{yx,x}$ and $p_{,y} = 0$. That means $p = p(x)$. Finally from equilibrium equation, we get $\sigma_{xy,y} = p_{,x} = \text{constant}$. Integration using given pressure at inlet and outlet will provide

$$p = \frac{p_{out} - p_{in}}{2L}x + \frac{p_{in} - p_{out}}{2} \quad (32)$$

Then

$$\sigma_{xy,y} = \frac{\partial}{\partial y} \left\{ \eta \frac{\partial v_x(y)}{\partial y} \right\} = \frac{p_{out} - p_{in}}{2L} \quad (33)$$

Integrating we obtain

$$\eta \frac{\partial v_x(y)}{\partial y} = \frac{p_{out} - p_{in}}{2L} y + A \quad (34)$$

The problem is symmetric along the x axis, at the center ($y=0$), $\frac{\partial v_x(y)}{\partial y} = 0$ give $A = 0$.

For Newtonian fluid ($\eta = constant$), by integrating and using no slip condition ($v_x = 0$ at $y = \pm H$). Finally the solution will be

$$v_x(y) = \frac{p_{in} - p_{out}}{4L} \left(\frac{H^2 - y^2}{\eta} \right) \quad (35)$$

For Power-law fluid which the viscosity is not a constant anymore but a function of equivalent strain rate $D_{eq} = \sqrt{2\underline{\underline{D}} : \underline{\underline{D}}}$. It is usually written as $\eta(D_{eq}) = \eta_0 D_{eq}^{(m-1)}$. Integrating from (33)

$$\eta_0 \left(\frac{\partial v_x}{\partial y} \right)^{m-1} \frac{\partial v_x}{\partial y} = \frac{p_{out} - p_{in}}{2L} y$$

$$\eta_0 \left(\frac{\partial v_x}{\partial y} \right)^m = \frac{p_{out} - p_{in}}{2L} y$$

$$\frac{\partial v_x}{\partial y} = \left(\frac{p_{out} - p_{in}}{2L\eta_0} y \right)^{1/m}$$

The solution can be found by integrating with the boundary condition at the top and bottom of the tube:

$$v_x = \left(\frac{p_{in} - p_{out}}{2L\eta_0} \right)^{1/m} \left(\frac{H^{\frac{1}{m}+1} - |y|^{\frac{1}{m}+1}}{1/m+1} \right) \quad (36)$$

- **Numerical solutions**

The simulations of the poseuille flow in rectangular pipe of 2x2 m ($H = 1$ m) cross section and 6 m ($L = 3$ m) long were done in X-FEM to compare with the analytical solutions. In the X-FEM code, we cannot directly impose given pressure at the inlet and outlet of the pipe. The traction forces were used instead by the relation $\underline{t} = p\underline{n}$. The fluid viscosity used in the simulation is $0.002 Pa \cdot s$. In addition, power law index of 0.3 was used in power law fluid case. Two different meshes were applied in this simulation as shown in the figure C.9.

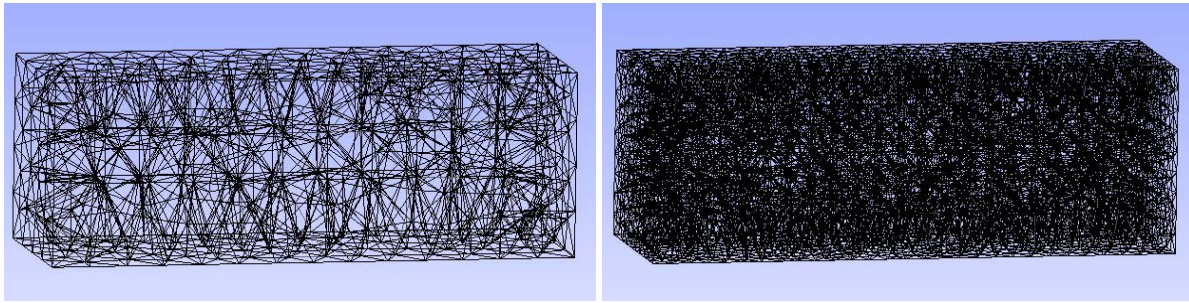


Figure C.9: Poiseuille flow test case: coarse mesh (left) and fine mesh (right)

- Newtonian Fluid

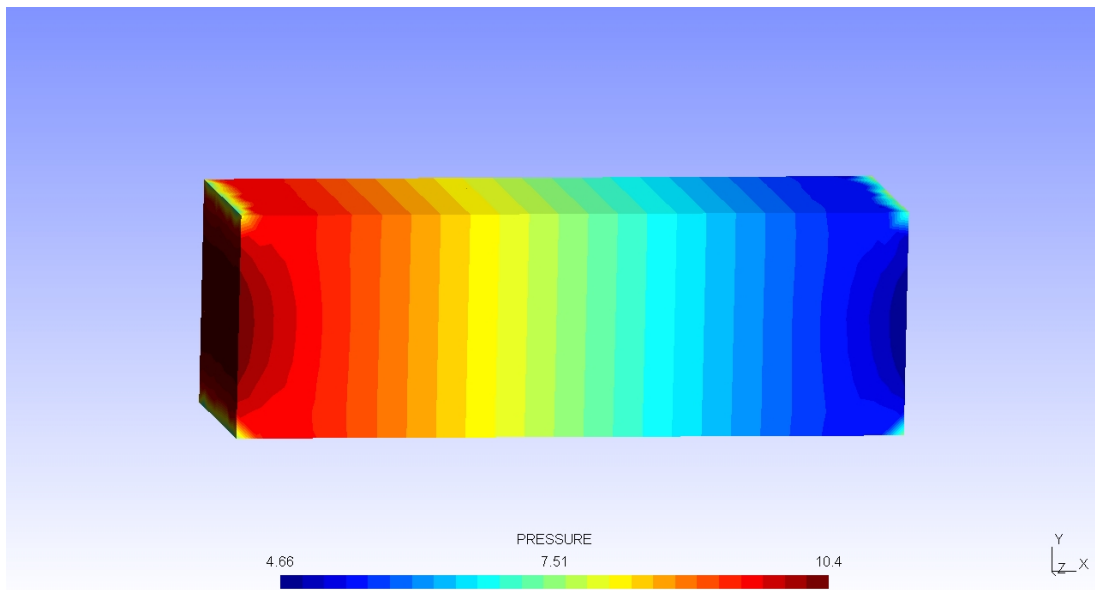


Figure C.10: Poiseuille flow test case result (Newtonian fluid): Pressure distribution

The pressure distribution computed from X-FEM with fine mesh is shown in figure above. The distribution looks perfectly linear, as expected, except at the top and bottom edge of inlet and outlet of the tube. This was expected because of the Neumann's type boundary conditions imposed at the inlet and the outlet. The pressure along the tube can be extracted from computational results and plotted. Figure C.11 shows pressure distribution along the tube (x axis) at location $y=0$ and $z=0$ of both coarse and fine meshes compare with analytical solution. The edge effect gives little underestimated pressure at the inlet and overestimated at the outlet.

The velocity profile of the flow can be also plotted as shown in the Figure C.12. The velocity along y axis at location $x=0$ and $z=0$ of the coarse mesh and fine mesh are compared. The coarse mesh solution is underestimated and cannot represent good shape of velocity profile at the center of the tube where the convexity is occurred. The finer mesh improved result of the computation. It gives nearly the same as analytical solution.

Figure C.13 shows the different velocity profile at different location of the fine mesh solution, $x=0$, $x=1$ and $x=2.8$ with $z=0$. The graph of location $x = 2.8$ which is near the outlet edge deliver slightly higher error while the result of location $x=0$ and $x=1$ giving the same result.

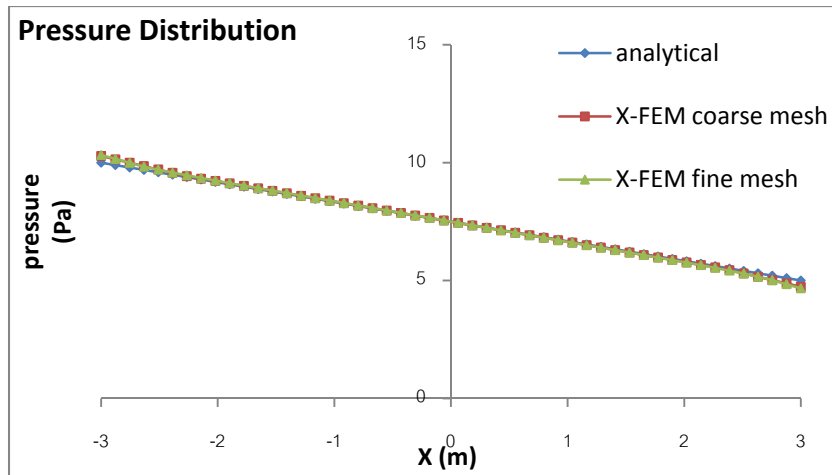


Figure C.11: Poiseuille flow test case result (Newtonian fluid): Pressure distribution

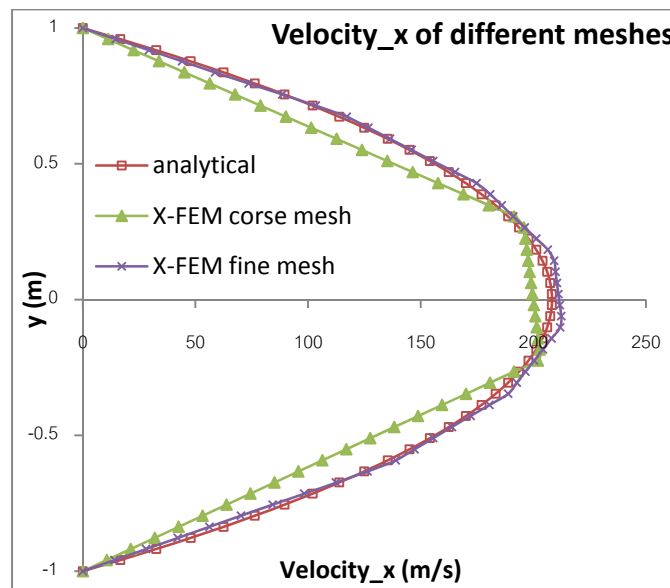


Figure C.12: Poiseuille flow test case result (Newtonian fluid): Velocity profiles of different meshes

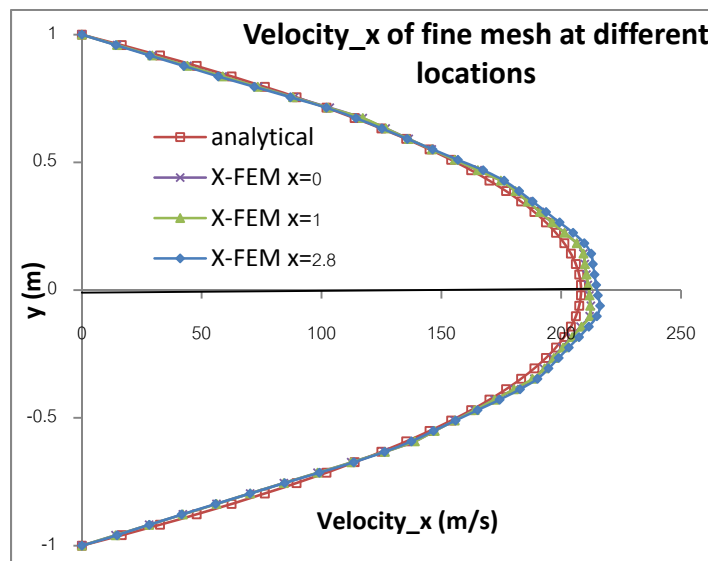


Figure C.13: Poiseuille flow test case result (Newtonian fluid): Velocity profiles of fine mesh extracted from different locations

- Power law fluid

The X-FEM solutions of power law fluid which is non-linear problem are shown in Figure C.14. Coarse mesh gave poor result but result from fine mesh is acceptable.

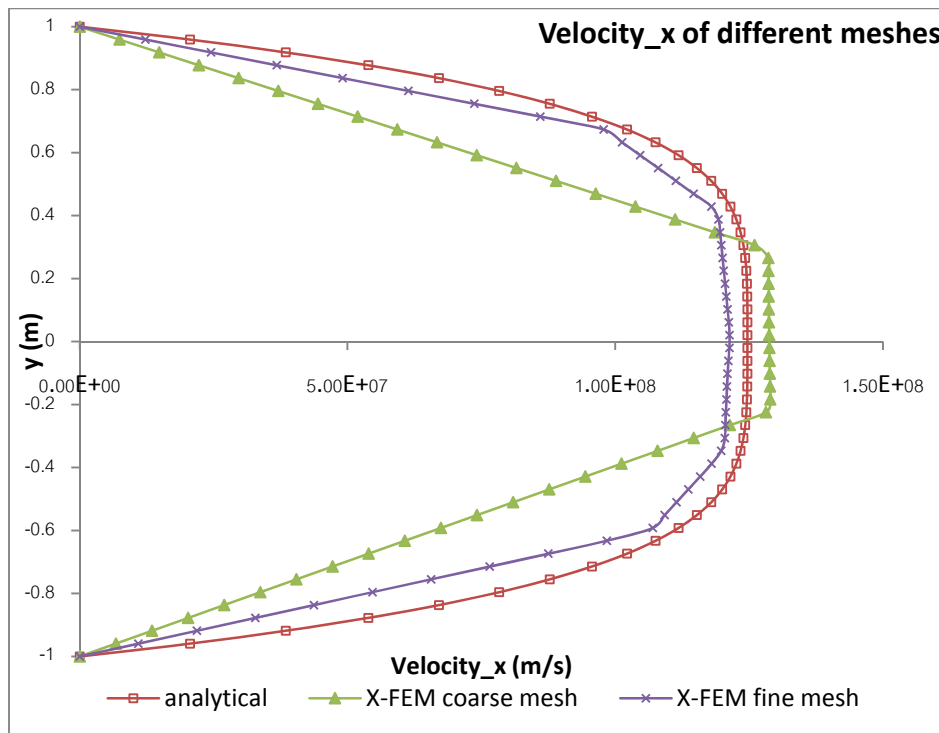


Figure C.14: Poiseuille flow test case result (Power-law fluid): Velocity profiles of different meshes

Remark that concerning the velocity profiles obtained in figures C.12, C.13 and C.14, results sometimes look really poor compared to the apparent number of point represented on the concerned graphs. The number of plotted points does not correspond to the number of elements, results are just “over-sampled” for representation purpose. Looking at coarse meshes results, one clearly sees that there are only about 3 elements in the thickness whereas there are 6 for the so-called fine mesh. Furthermore, GMSH does not represent properly order two function so that we only observe linear evolutions over each element. The real solution is obviously much better than the one represented here.

2.3) Poiseuille flow with free surface test case

In this case, simulation of the poiseuille flow in the same tube as last test case has been done but with different boundary condition and using two Newtonian fluids. The interface of two materials is located at plane $x = -0.5$ with properties as shown in figure below.

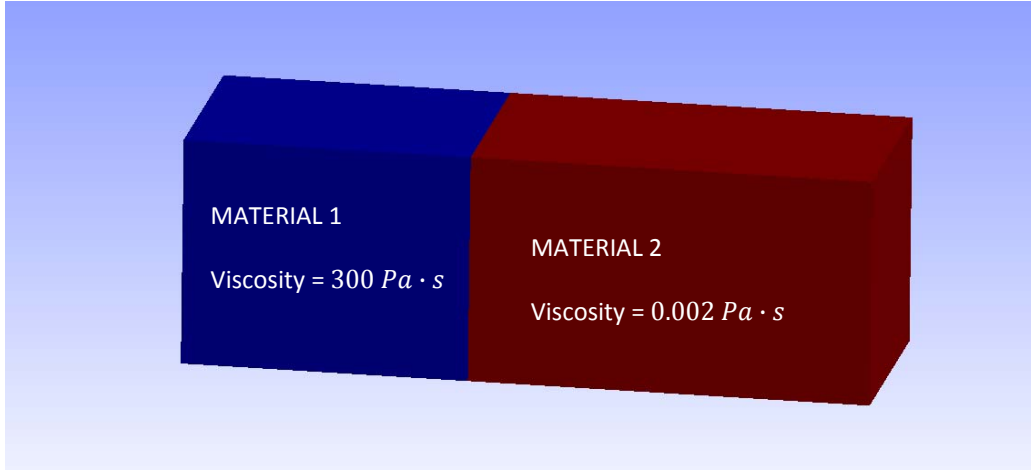


Figure C.15: Poiseuille flow with free surface test case

Additional boundary conditions are $v_x = 0 \text{ m/s}$ at front and back side of the tube instead of inviscid flow condition. These made the problem to be full 3D problem. Free surface of two materials is represented by level set in X-FEM simulation. The tractions (pressure) apply at the left and right sides of the tube are 10 and 0 Pa respectively. The problem is transient or time dependant. When time increase, free surface will be propagated. At each time step, the solution of velocities and pressure were given to equation (29) by solving fluid flow equations. Evolution of the free surfaced then can be solved. Even though we do not have analytical solution of this problem, it is interesting to test whether the numerical results conserve flow conservation law. To do this we will compute the volume of material 1 by two methods.

First method, using

$$V_n = V_0 + \frac{(Q_{n-1} + Q_n)}{2} \times \Delta t \quad (37)$$

where V_0 is initial volume, $Q_n = \iint_{S_{in}} \underline{v} \cdot dS$ is volumetric flow rate, Δt is time step.

Q_n was calculated in gmsh post processing by cut only plane $x = -3 \text{ m}$ of v_x exported result and then integrated over the domain.

Second method is

$$V_n = \iiint_V \chi_n dV \quad (38)$$

where χ_n is iso-zero of the level set.

However the second method was not done directly, it was approximated in post processing process by using extract plug-in to extract only material 1 and then used integrate plug-in to find volume.

The results of simulation using constant time step $\Delta t = 20 \text{ s}$ can be shown in the table below. It is shown that the different of volume computed by both methods is less than 4%

| Step (n) | t_n | Q_n | V_n First method | V_n Second method | Percentage difference |
|----------|-------|---------|-----------------------|------------------------|-----------------------|
| 1 | 20 | 0.00749 | 10.15 | 9.81 | 3.40 |
| 2 | 40 | 0.00743 | 10.30 | 10.40 | 0.98 |
| 3 | 60 | 0.00735 | 10.45 | 10.50 | 0.51 |
| 4 | 80 | 0.00722 | 10.59 | 10.60 | 0.07 |
| 5 | 100 | 0.00712 | 10.74 | 10.70 | 0.33 |
| 6 | 120 | 0.00705 | 10.88 | 11.00 | 1.12 |
| 7 | 140 | 0.00699 | 11.02 | 11.10 | 0.74 |
| 8 | 160 | 0.00693 | 11.16 | 11.30 | 1.27 |
| 9 | 180 | 0.00684 | 11.29 | 11.50 | 1.80 |
| 10 | 200 | 0.00674 | 11.43 | 11.60 | 1.47 |
| 11 | 220 | 0.00665 | 11.56 | 11.70 | 1.16 |
| 12 | 240 | 0.00658 | 11.70 | 11.90 | 1.72 |
| 13 | 260 | 0.00651 | 11.83 | 12.00 | 1.45 |
| 14 | 280 | 0.00644 | 11.96 | 12.10 | 1.19 |
| 15 | 300 | 0.00637 | 12.09 | 12.10 | 0.12 |
| 16 | 320 | 0.00631 | 12.21 | 12.40 | 1.53 |
| 17 | 340 | 0.00625 | 12.34 | 12.50 | 1.31 |
| 18 | 360 | 0.00619 | 12.46 | 12.70 | 1.89 |
| 19 | 380 | 0.00613 | 12.59 | 12.80 | 1.69 |
| 20 | 400 | 0.00606 | 12.71 | 12.90 | 1.51 |
| 21 | 420 | 0.00600 | 12.83 | 13.10 | 2.10 |
| 22 | 440 | 0.00594 | 12.95 | 13.20 | 1.93 |
| 23 | 460 | 0.00588 | 13.07 | 13.30 | 1.78 |
| 24 | 480 | 0.00583 | 13.18 | 13.60 | 3.12 |
| 25 | 500 | 0.00578 | 13.30 | 13.70 | 2.97 |
| 26 | 520 | 0.00573 | 13.41 | 13.80 | 2.84 |
| 27 | 540 | 0.00568 | 13.53 | 13.80 | 1.99 |
| 28 | 560 | 0.00563 | 13.64 | 13.90 | 1.88 |
| 29 | 580 | 0.00558 | 13.75 | 14.00 | 1.78 |
| 30 | 600 | 0.00553 | 13.86 | 14.20 | 2.39 |
| 31 | 620 | 0.00548 | 13.97 | 14.30 | 2.30 |
| 32 | 640 | 0.00544 | 14.08 | 14.50 | 2.91 |
| 33 | 660 | 0.00539 | 14.19 | 14.80 | 4.20 |
| 34 | 680 | 0.00534 | 14.30 | 14.90 | 4.12 |
| 35 | 700 | 0.00530 | 14.41 | 14.90 | 3.37 |
| 36 | 720 | 0.00526 | 14.51 | 15.00 | 3.31 |
| 37 | 740 | 0.00522 | 14.62 | 15.10 | 3.26 |
| 38 | 760 | 0.00518 | 14.72 | 15.10 | 2.55 |
| 39 | 780 | 0.00514 | 14.82 | 15.40 | 3.82 |
| 40 | 800 | 0.00510 | 14.93 | 15.50 | 3.78 |

Table C.1: Poiseuille flow with free surface test case result: Volume of material 1 at each time step

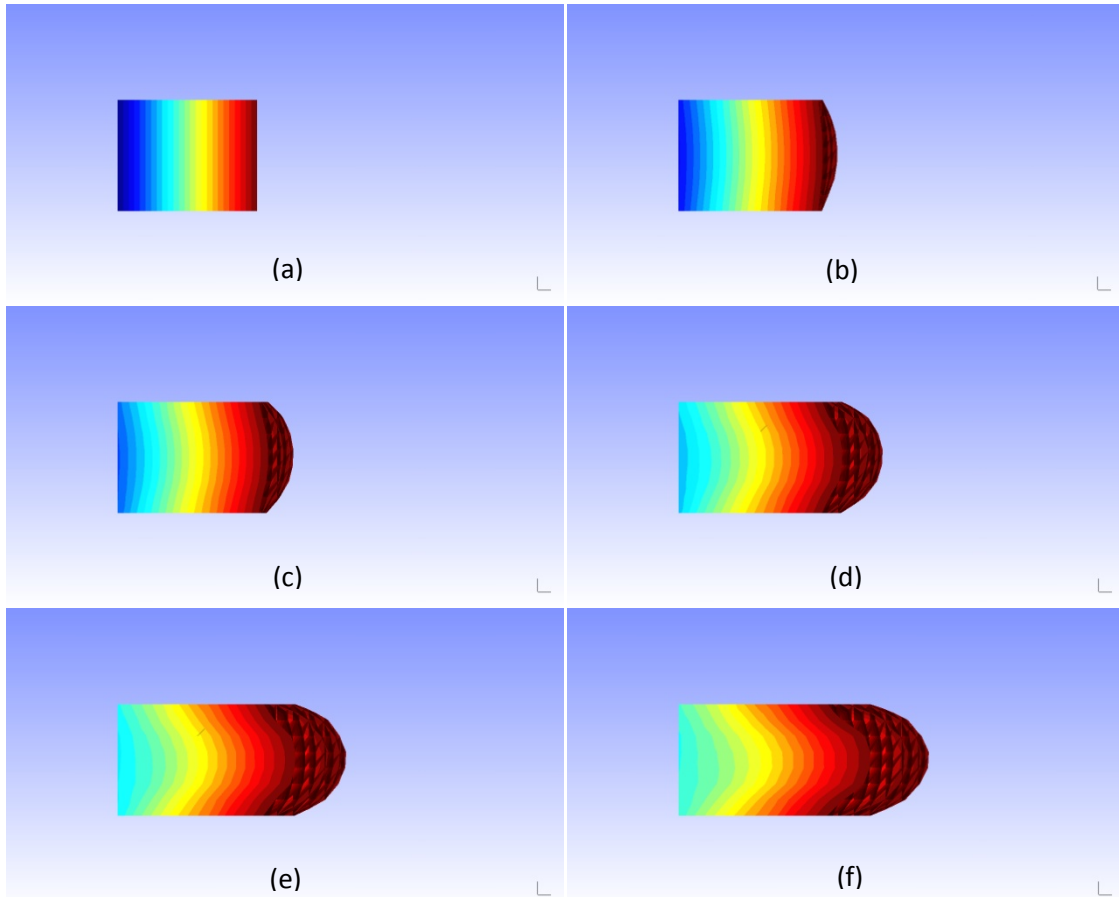


Figure C.16: Poiseuille flow with free surface test case result: Level set propagation (Material 1 part only)

(a) $t = 0$ s, (b) $t = 100$ s, (c) $t = 200$ s, (d) $t = 400$ s, (e) $t = 600$ s (f) $t = 800$ s

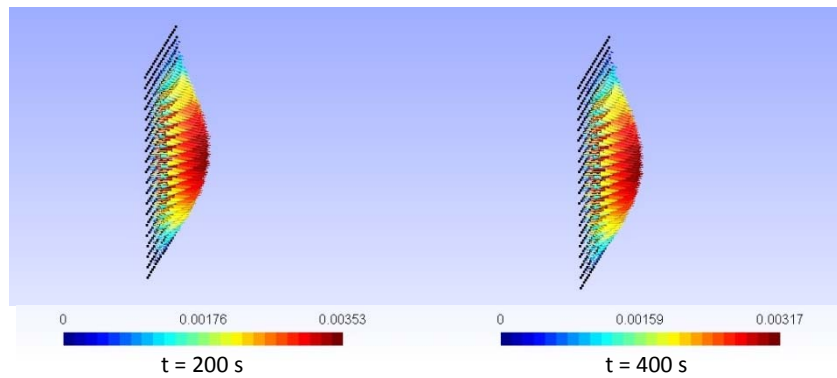


Figure C.17: Poiseuille flow with free surface test case result: Velocity profile at plane $x = -3$ m at $t = 200$ and 400 s

3) Thermal test case

3.1) Steady state conduction test case

We will observe heat transfer in a 2x2 m square cross section bar with length of 4 m which contain two different materials having constant thermal conductivity 0.1 and 1 $W/m \cdot K$. The interface of two materials is located at the center of the bar. Fixed temperature are given at right and left side of the bar equal to 10 and 50 $^{\circ}C$ respectively. By assigning no heat flux on the top and bottom and without heat source, the 3-D problem becomes 1-D problem (in x direction).

The analytical solution can be found by solving equation (28.5) in steady state (*which* $\rho c \dot{T} = 0$) separately in material 1 and 2 with condition that temperature at the interface is the same for both materials.

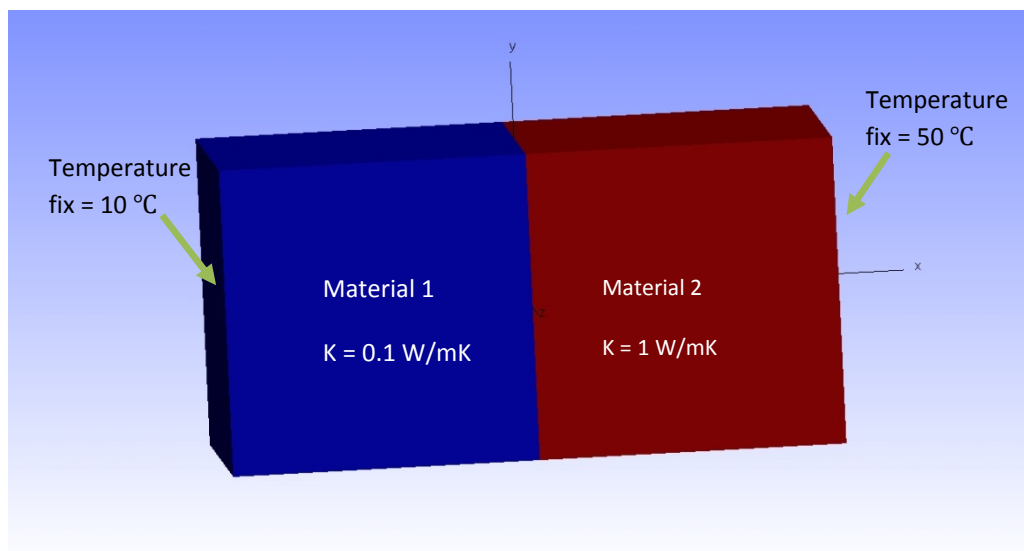
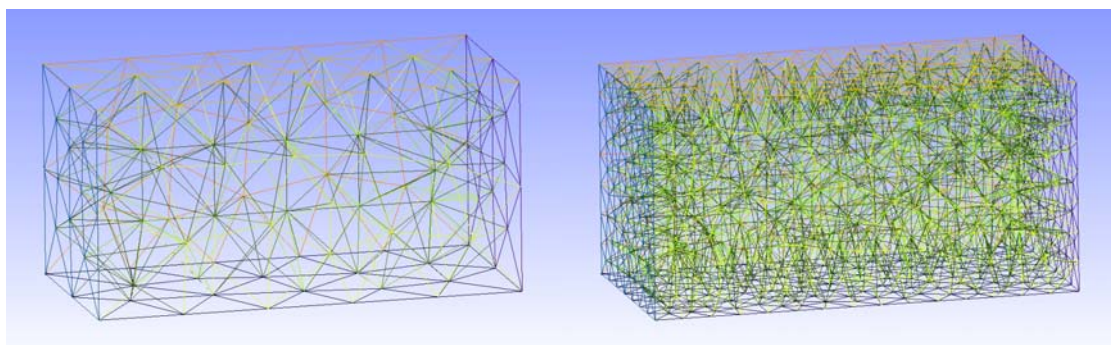
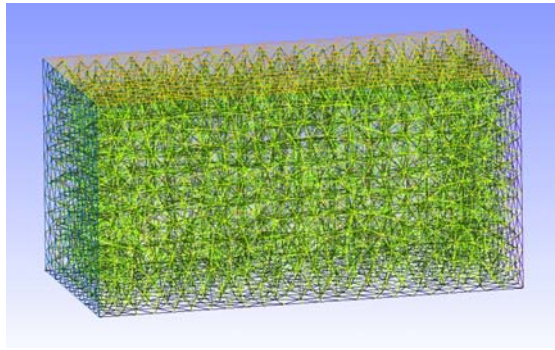


Figure C.18: Steady state conduction test case

The X-FEM computations were done in three different mesh sizes. Results compare very well to the analytical solution even form the coarse mesh as show in figure C.20. However, $\frac{\partial T}{\partial x}$ represented by coarse mesh cannot show good result near the interface of two materials where discontinuity of $\frac{\partial T}{\partial x}$ is occurred. This problem reduced when use finer meshes.



(a) Coarse mesh (b) Fine mesh
Figure C.19: Steady state conduction test case: different meshes



(c)Very fine mesh

Figure C.19: Steady state conduction test case: different meshes

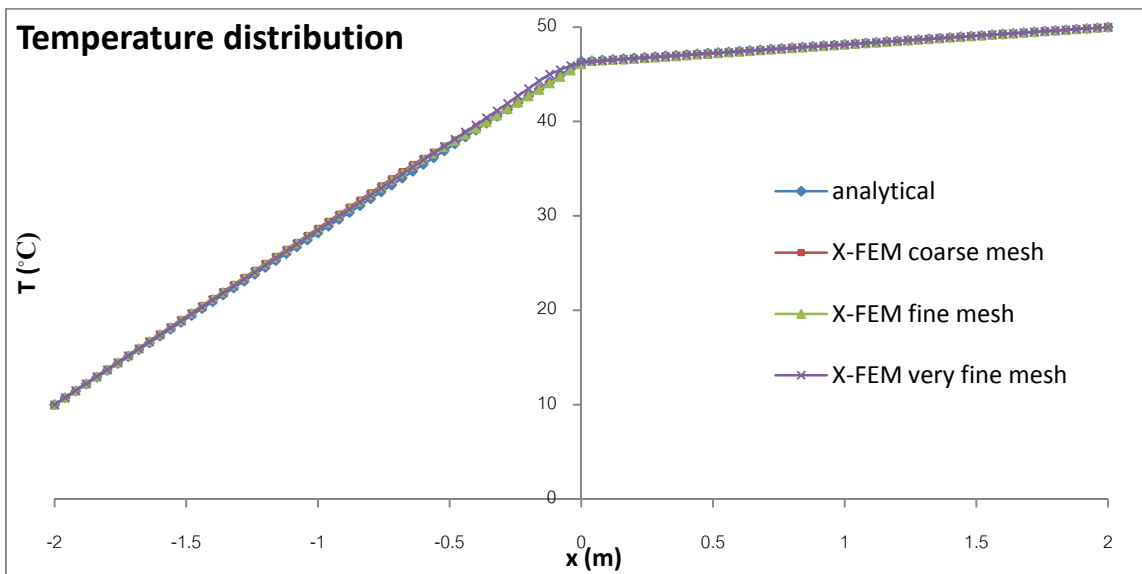


Figure C.20: Steady state conduction test case result: Temperature distribution

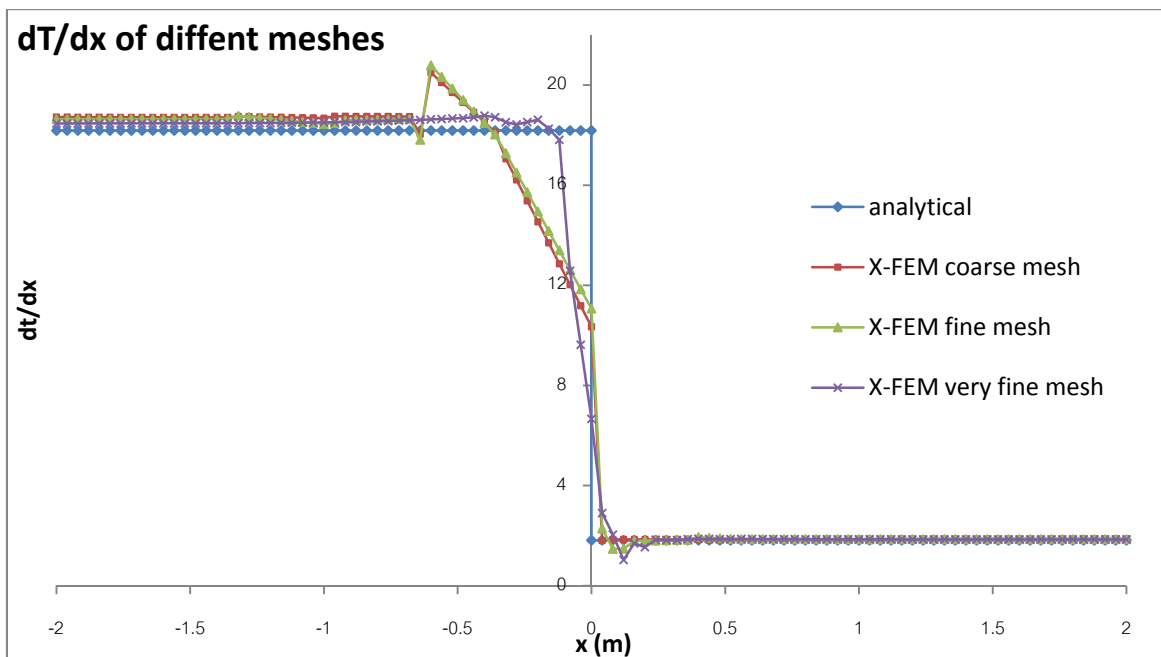


Figure C.21: Steady state conduction test case result: $\frac{\partial T}{\partial x}$ of different meshes

3.2) Transient conduction test case

For semi –infinite 1D bar with initial condition $T = T_i$, constant boundary condition $T = T_s$ at $x = 0$, solution is the error function:

$$\frac{T - T_s}{T_i - T_s} = \operatorname{erf}\left(\frac{x}{2\sqrt{\alpha t}}\right)$$

where $\alpha = \frac{k}{\rho c}$

with semi-infinite criterion:

$$\frac{L}{2\sqrt{\alpha t}} \geq 2$$

- Numerical solution

In 3D simulation, $0.5 \times 0.5 \text{ m}^2$ square cross section 8 m bar long was used. Initial temperature 0°C was set. Given temperature 10°C constant at $x = 0$. Temperature 0°C constant also had been given as a boundary condition at $x = 8 \text{ m}$ to make the problem satisfying semi-infinite characteristic. Backward Euler single step method, which is known to exhibit non-conditional stability, was use as a time integration technique. The results of the problem with $\alpha = 2.5 \times 10^{-4} \text{ m}^2/\text{s}$ can be shown below

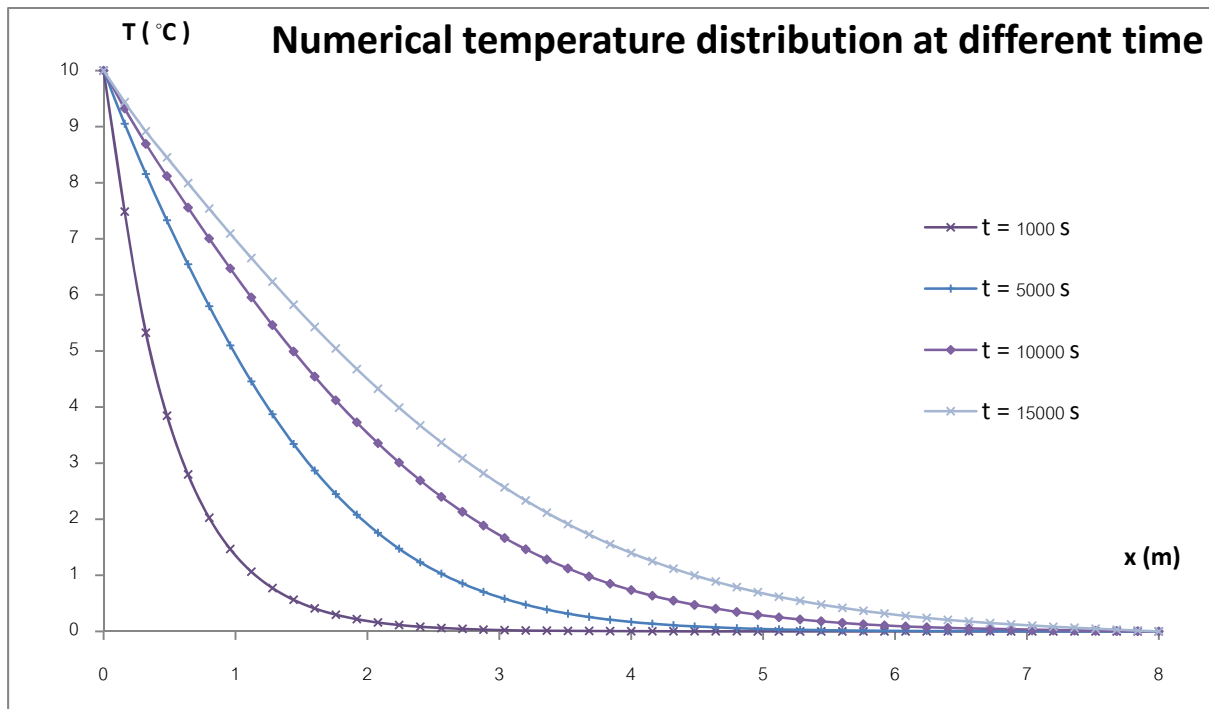


Figure C.22: Transient conduction test case result: Numerical temperature distribution at different time steps

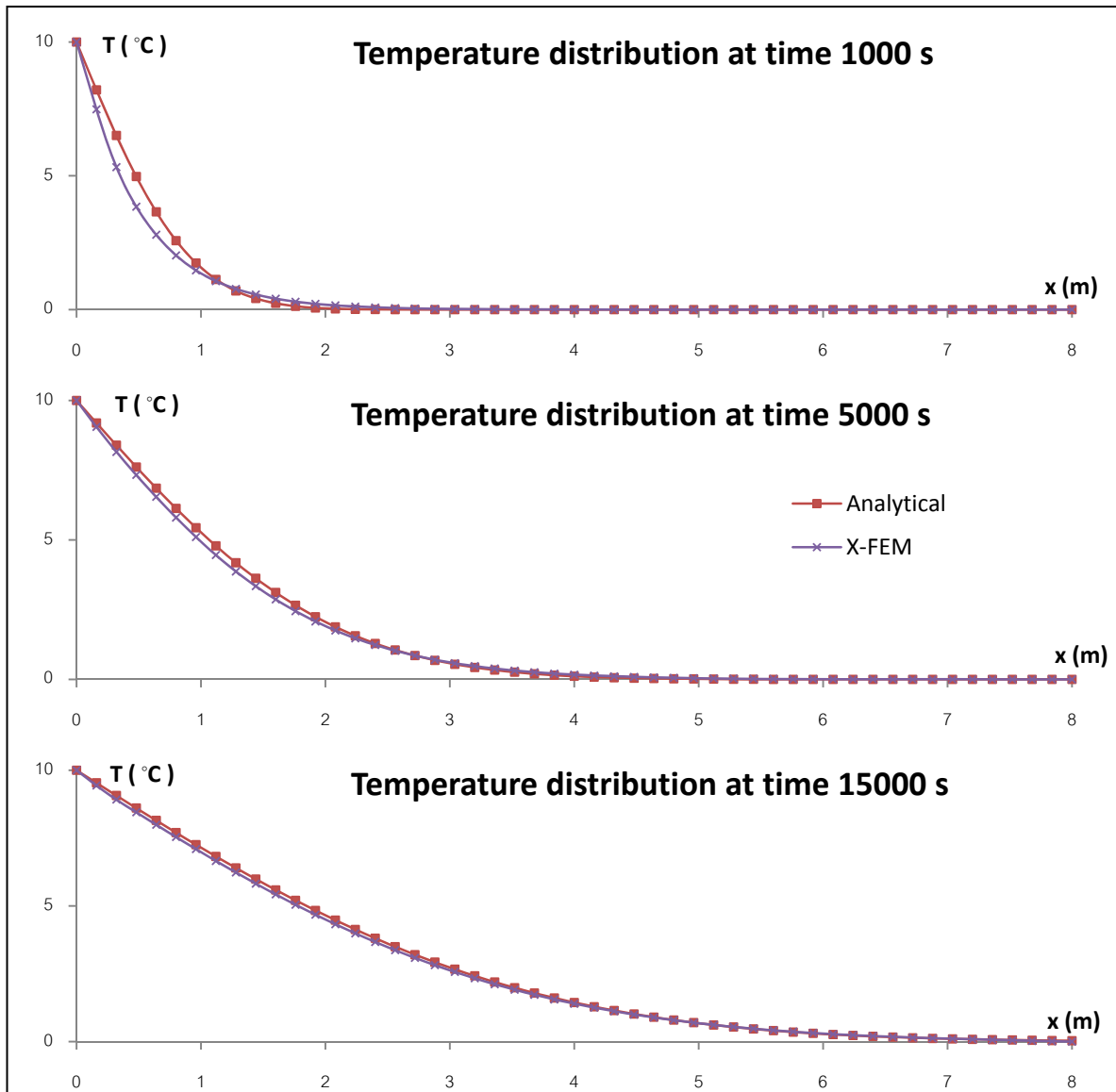


Figure C.23: Transient conduction test case result: Comparison of analytical and numerical solution

3.3 Steady state convection test case

Consider 1D steady state heat transfer problem, equation (28.1) then becomes

$$\rho c \frac{dT}{dx} \cdot v - k \frac{d^2T}{dx^2} = q_{gen} \quad (39)$$

With given boundary conditions, this ODE can be solved analytically.

The proposed test case is directly inspired from the one used by *Brooks and Hugues*. It was set using 2D 2x2m square domain where. Thermal capacity (ρc) = $1 \text{ J}/(\text{m}^3 \cdot \text{K})$, conductivity = 0.1, 1 and $100 \text{ W}/(\text{m} \cdot \text{K})$ were given for material properties. Heat source (q_{gen}) was constant and equal to $1 \text{ W}/\text{m}^3$, velocity was set to 2 m/s in +x direction. The initial and boundary condition temperature on the left and right sides of the domain equal to 0 K was prescribed. Temperature versus x position result extracted from central horizontal axis ($y=0$) can be plotted in figure C.24

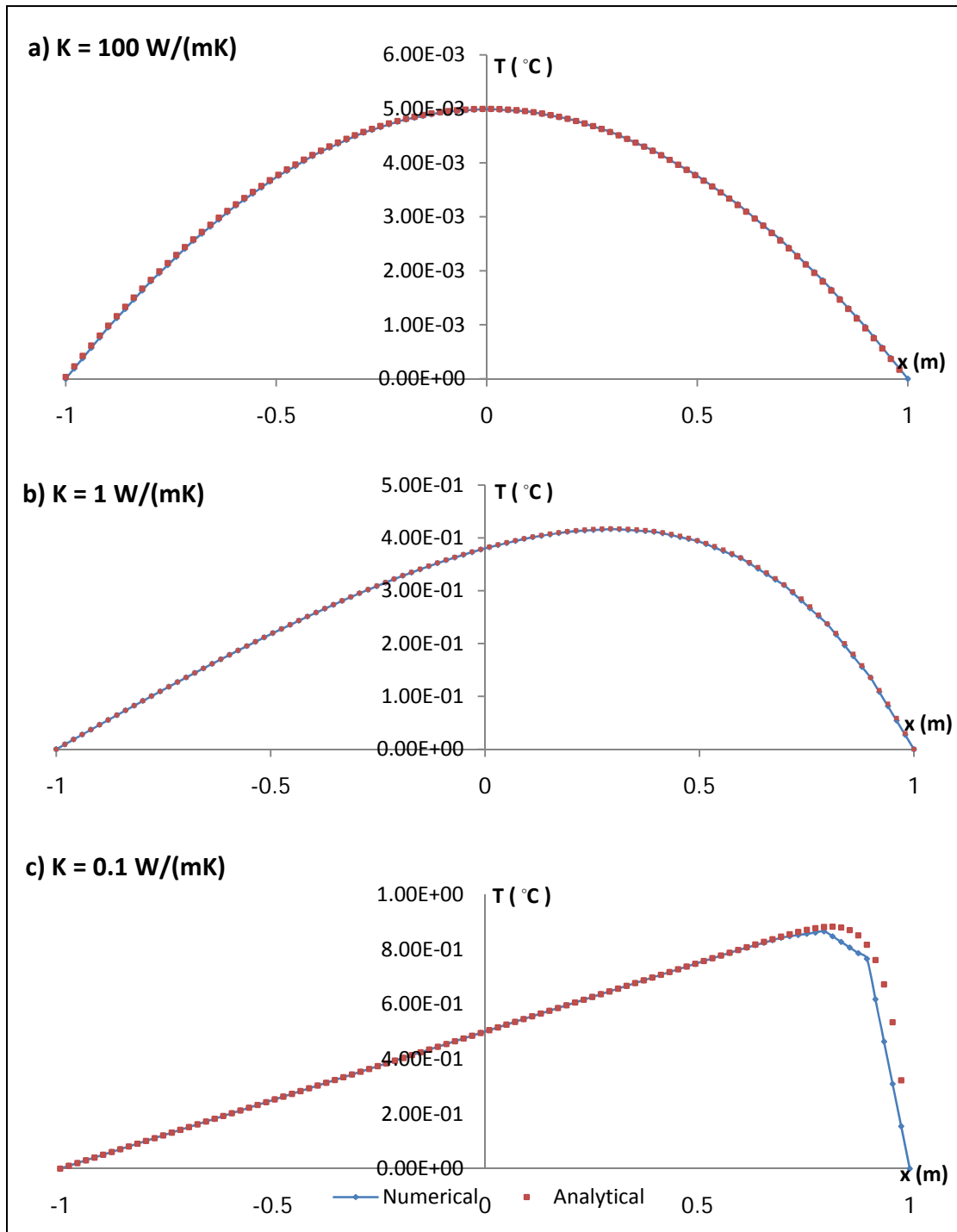
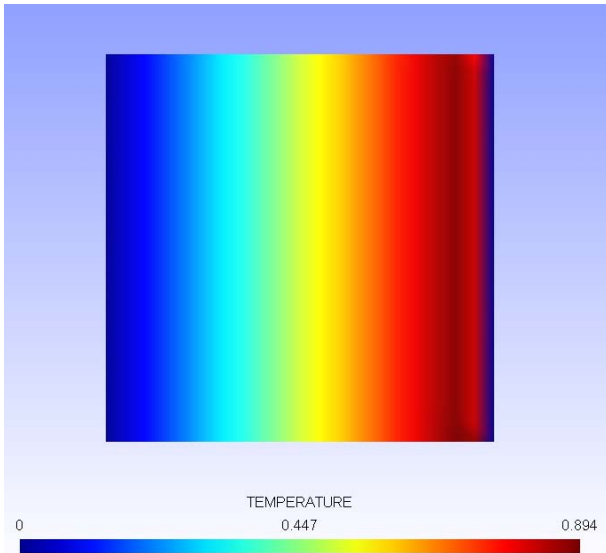
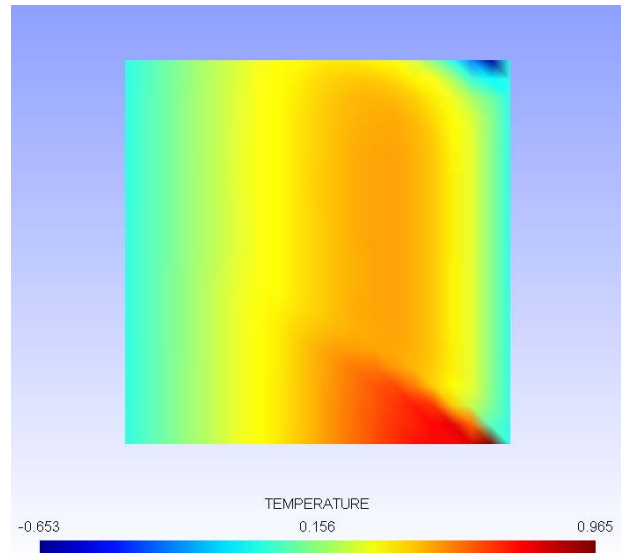


Figure C.24: Steady state convection test case result: Comparison of analytical and numerical solution with different thermal conductivity

The numerical solutions of convection problem using SUPG gave good results compare to analytical solutions. In case of high conductivity, the problem is dominated by diffusive term. The result shows as no convection occurred (figure C.24 a). Since the lower conductivity applied, velocity effects become important as shown in figure C.24 b) and c). The SUPG solution remains valid for very low conductivity or highly dominant convective term when classic Galerkin FEM exhibits spurious oscillations as shown in figure C.25.



a) SUPG



b) Galerkin

Figure C.25: Steady state convection test case result: SUPG and classical Galerkin FEM results with thermal conductivity = 0.005 W/(mK)

D. PROCESS SIMULATION

Geometry and Meshing

Three dimension rectangular box was set as a domain of simulation. Due to symmetry of the problem, only half of triangular energy director was represented by negative part of level set, also the partial of upper and lower welding parts. Air was prescribed in positive part of level set. The singularity at the tip of director has been smoothed. Since in this initial simulation, the problem was set to be 2D analysis in 3D domain, thickness of the domain does not take into account.

The meshes are made of unstructured tetrahedral elements over the whole domain. The finer refinement was used in the area near tip of the director where singularity might occur. Two meshes were set to compare the results.

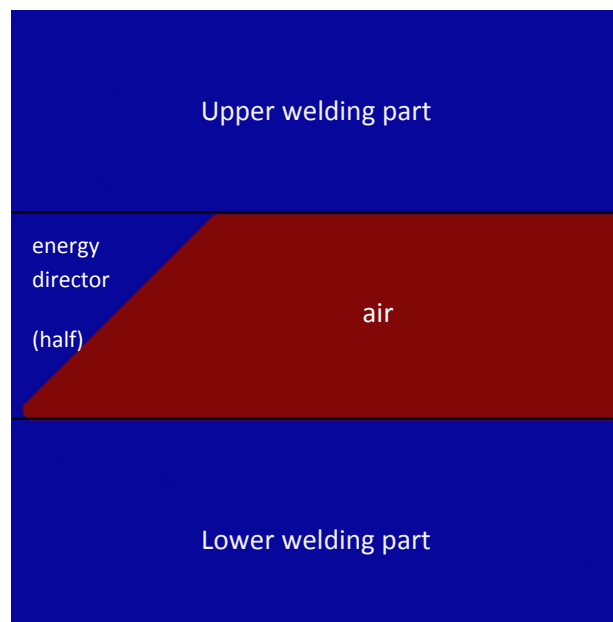
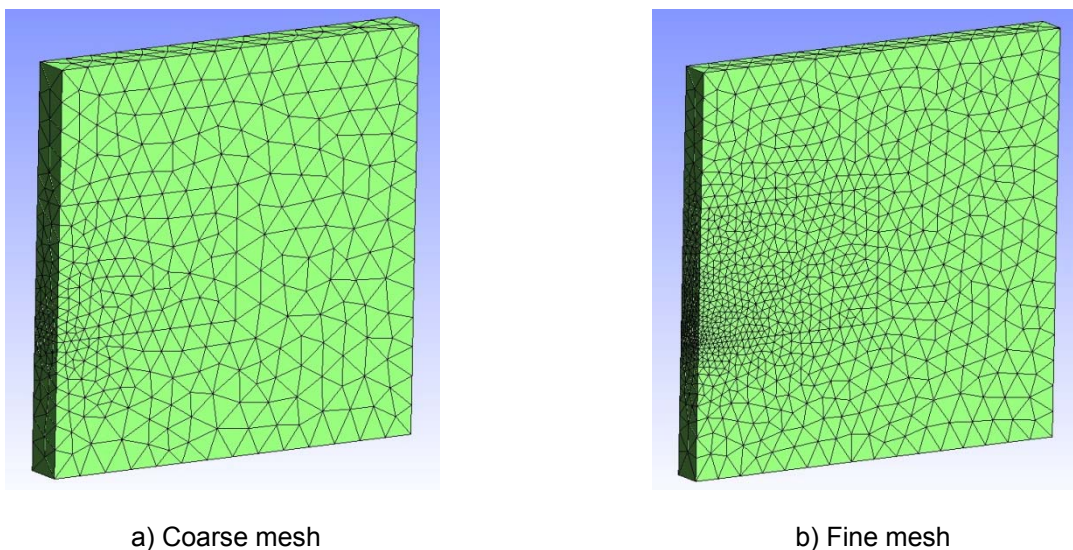


Figure D.1: Initial level set: negative part-blue, positive part-red



a) Coarse mesh

b) Fine mesh

Figure D.2: Meshing

Material Properties

For the elastic micro-chronological problem, the material was assumed to be isotropic. The young modulus was set as a function of temperature by using Arrhenius equation $E = E_0 e^{\left(\frac{16746}{RT}\right)}$ where R is gas constant. Poisson ratio was set to 0.49 to satisfy incompressibility.

The macro-chronological problem was set to pure viscous equations instead of visco-elastic for reasons invoked above. Power law was used as a constitutive equation. Newtonian viscosity was also set to be temperature dependant using Arrhenius equation.

The thermal conductivity and heat capacity were set to be constants. All material data can be found in table D.1

| | | |
|---------------------|----------------------|---|
| Elastic | Young modulus | $E = 6.26 \times 10^6 e^{\left(\frac{16746}{RT}\right)}$ Pa |
| | Poisson ratio | $\nu = 0.49$ |
| Viscous flow | Newtonian viscosity | $\eta_0 = 14.11 e^{\left(\frac{33731}{RT}\right)}$ Pa · s |
| | Power index | $m = 0.5$ |
| Thermal | Heat capacity | $\rho c = 2.6 \times 10^6$ J/m ³ · K |
| | Thermal conductivity | $K = 0.25$ W/m · K |

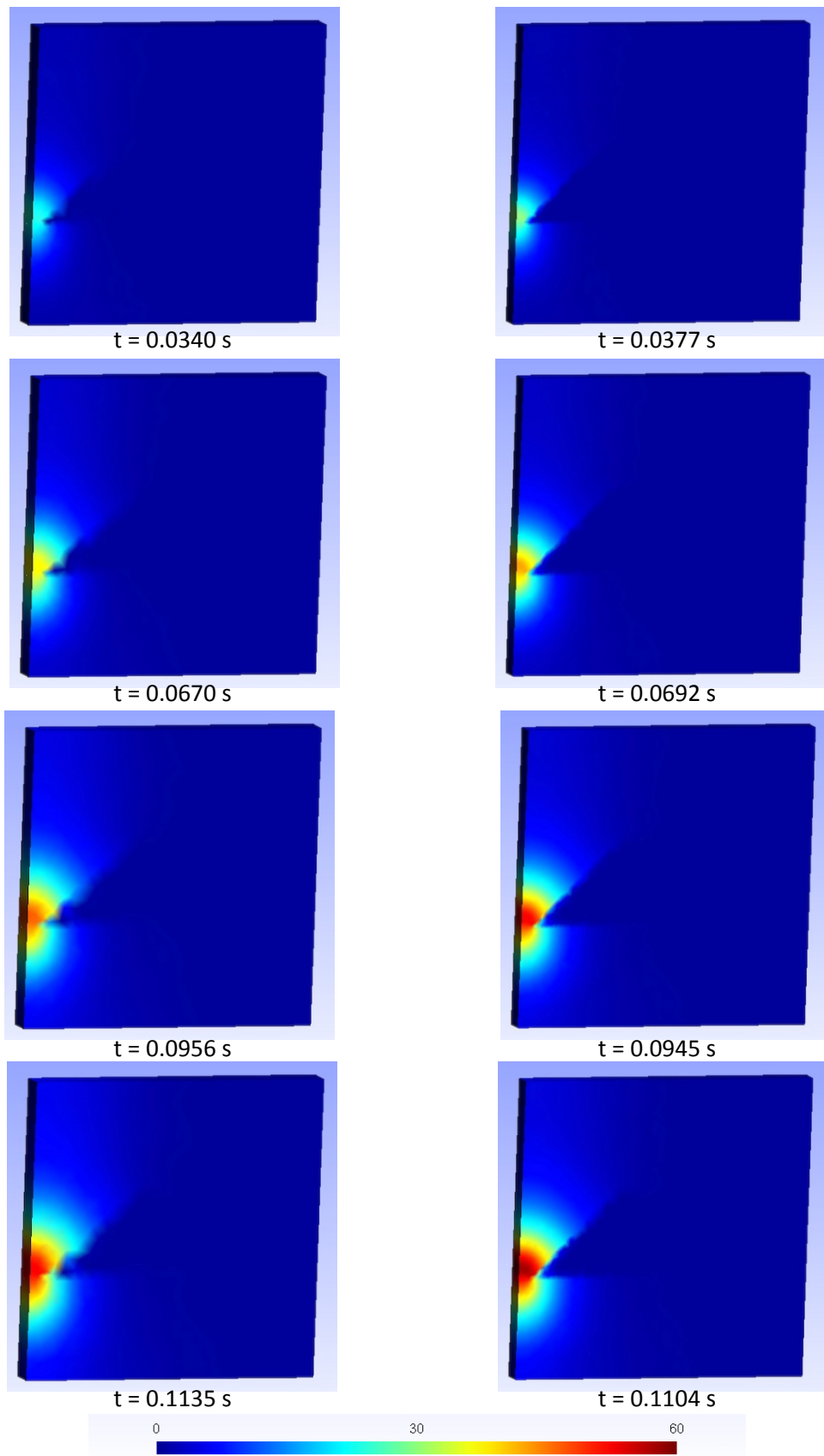
Table D.1: Material data

Boundary and initial condition

For macro-chronological viscous system, the constant velocity was applied on the top of the mesh in assumption that overall welding process time is two seconds. The evolution of displacement which is linear in time was also applied to match that assumption for micro-chronological elastic problem. The bottom of the part was fixed. Left side boundary condition was set to sliding condition in y direction due to symmetric of the system. Since the simulation was set as 2D, zero velocity and displacement in outward direction (z direction) of front and back surfaces was prescribed. The thermal boundary conditions are no heat flux in all boundaries. Initial temperature was set to 0 °C which is not realistic.

Results and Discussion

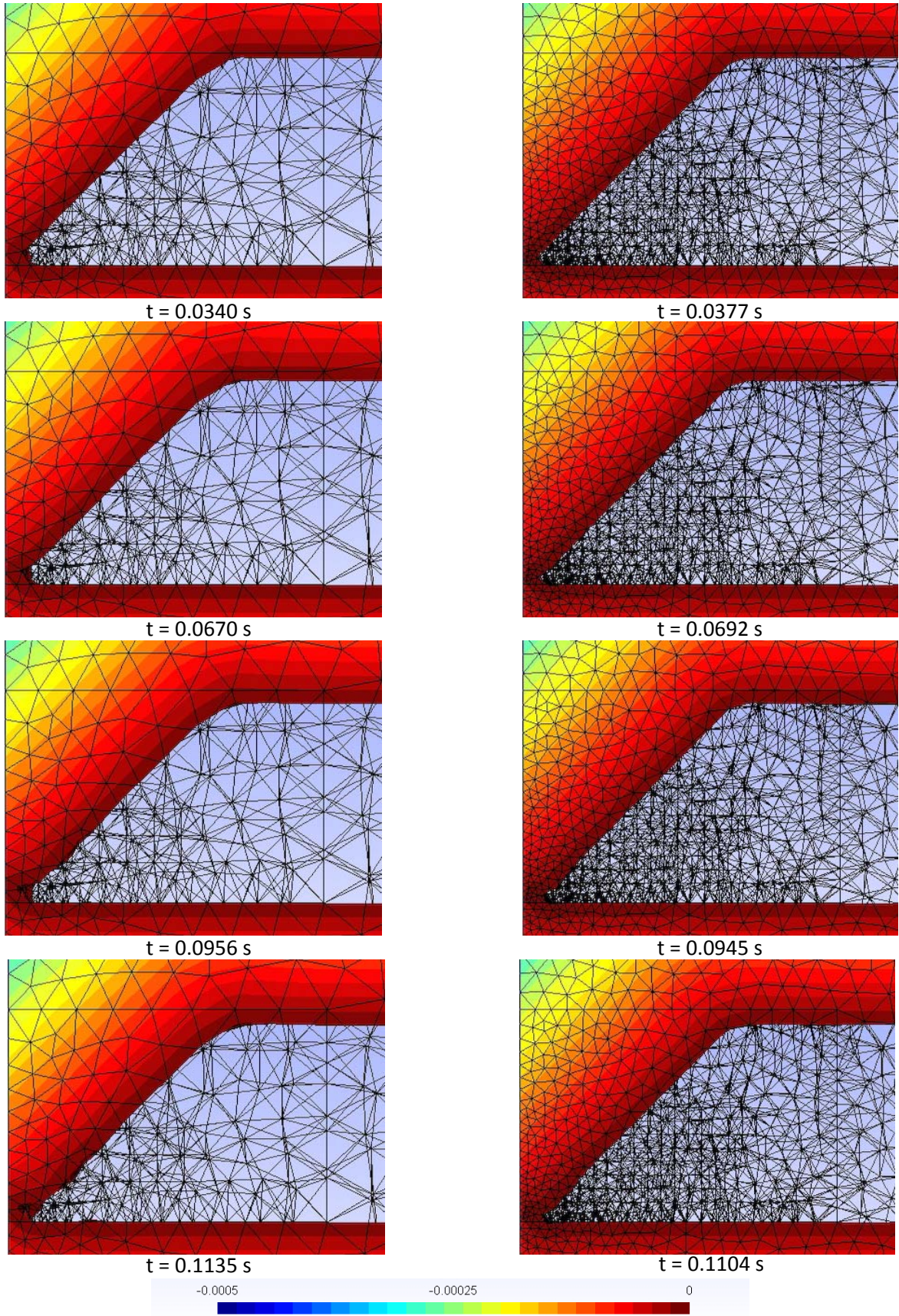
The comparisons of results of the computation can be observed in figure D.3. and D.4. The results show that flow of the director was began at the tip of the director. This is coinciding with temperature distributions which also show that it was heat first at the tip. This is in agreement with theoretical. The comparisons cannot be done at the same time of the process. This is because time steps for each simulation are under constraint of CFL condition which depends on element size. The closest times were chosen to compare. It is obvious to see that fine mesh gave better results.



a) Coarse mesh results

b) Fine mesh results

Figure D.3: Process simulation results: Temperature distribution comparison



a) Coarse mesh results

b) Fine mesh results

Figure D.4: Process simulation results: Evolution of level set comparison

Although computation gave good results at the beginning, “bus error” which is about memory problem occurred randomly during the simulation. The error occurred sooner as the size of the problem increase. For coarse mesh problem can reach around 60th time step of the computation while fine mesh can reach only around 20th step. Further results of coarse mesh can be found in figure D.5. and D.6. The free surface evolutions show that lower welding part started to deform at $t = 0.4$ s when the level set flowed beyond local fine mesh region. Finer mesh would be needed to observe better result.

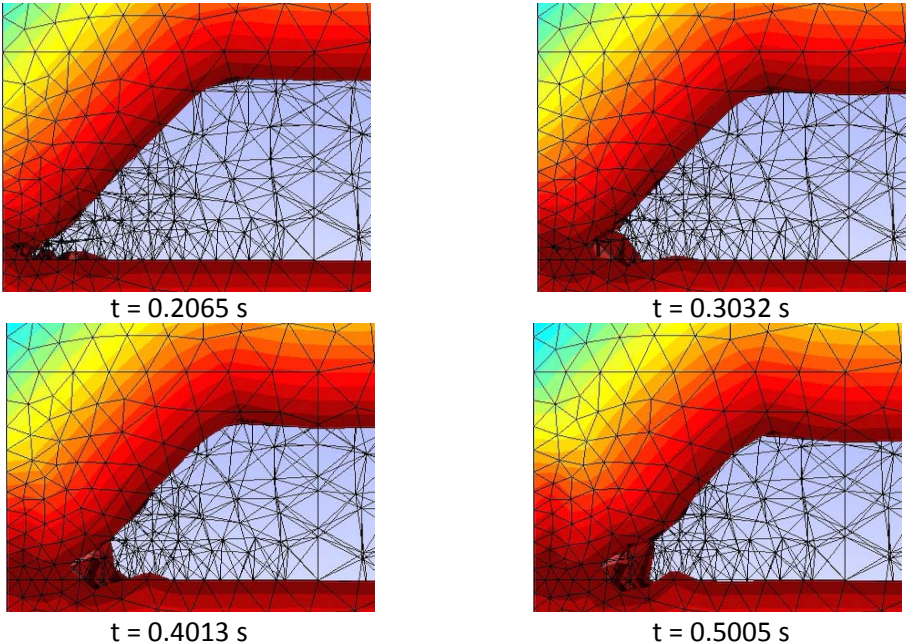


Figure D.5: Process simulation results: Coarse mesh - evolution of level set

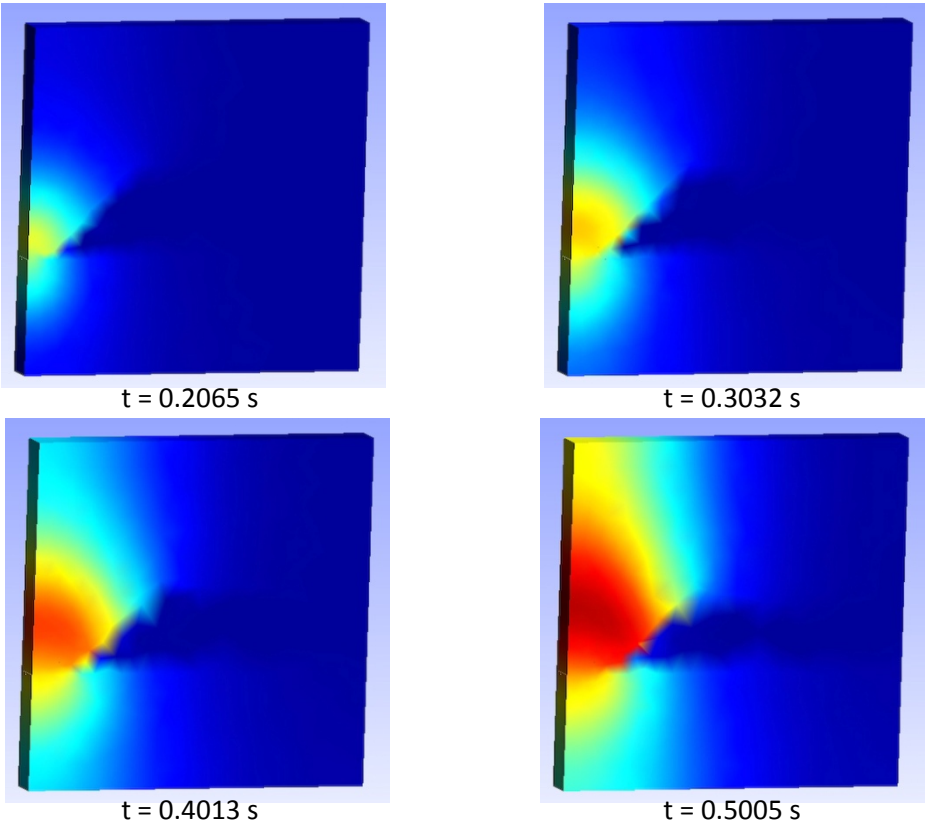


Figure D.6: Process simulation results: Coarse mesh – temperature distribution

E. CONCLUSION

The method of time homogenization allows us to split complex thermo-mechanical problem into coupled problem of simple two mechanical problems in different time scales and one thermal problem. Three systems of equations can be treated separately. The macro-chronological elastic problem is solved to induce heat source for solving thermal problem. Solving thermal problem will update material parameters which are temperature dependent. Macro chronological visco-elastic is simplified to pure viscous problem gives geometry evolution during the process.

The extension of 2D simulation to 3D was successfully done, especially for three single physics as mention above. A number of necessary test cases had been done for validation of the C++ Library X-FEM code. It showed good results for each problem.

The final simulations of the ultrasonic process are in agreement with theoretical. Unfortunately, the simulation cannot run until the end of the process because problem of memory allocation. Since the errors happened at random point with the same simulation and occurred sooner when size of the problem is increased, this supposes to be physical memory problem which could not be solved.

However, to simulate “fully 3D dynamic” ultrasonic welding process which the sonotrode is moving along the length of the director that performed as a weld line, the thickness of the system must be much thicker than one used in this test. More resources of the machine will be need or in another way is to perform parallel computation. Also, the method to imposed moving boundary conditions (to represent moving sonotrode) must be studied further.

F. REFERENCES

A. Levy, A. Poitou, S. Le Corre and E. Soccard, "Ultrasonic Welding of Thermoplastic Composites, Modeling of the Process", *International Journal of Material Forming*, 1:887-890, 2008

Anton Smolianski, "Finite-element/level-set/operator-splitting (FELSOS) approach for computing two-fluid unsteady flows with free moving interfaces", *International Journal for Numerical Methods in Fluids*. 48(3):231-269, 2004

William R. Oates, "Welding Handbook Volume 3", Miami, American welding society, 1997

Jean Donea and Antonio Huerta, "Finite Element Methods for Flow Problems", West Sussex, John Wiley & Sons Ltd., 2003

Montgomery T. Shaw and William J. MacKnight, "Introduction to Polymer Viscoelasticity", New Jersey, John Wiley & Sons Ltd., 2005

I. Babuska, "The Finite Element Method with Lagrangian Multipliers." *Numerische Mathematik*, 20:179-192, 1973

A. N. Brooks and T.J.R. Hughe, "Streamline upwind/Petrov-Galerkin Formulations for Convection Dominated Flows with particular emphasis on the incompressible Navier-Stokes Equations", *Comput. Methods Appl. Mech. Eng.*, 32:199-259, 1982.

Erwin Kreyzig, "Advance Engineering Mathematics", John Wiley & Sons Ltd., 2006.

Jacob Fish, Ted Belytschko, "A First Course in Finite Elements", John Wiley & Sons Ltd., 2007.

Avraham Benatar, Raman V. Eswaran and Satinder K. Nayar, "Ultrasonic welding of thermoplastics in the near-field", *Polymer Engineering and Science*, 29(23):1689 – 1698, 2004.

C.J. Nonhof and G.A. Luiten, "Estimates for process conditions during the ultrasonic welding of thermoplastics", *Polymer Engineering and Science*, 36(9):1177-1183, 2004.